

GIANTS IN THE LOCAL REGION

R. EARLE LUCK¹ AND ULRIKE HEITER²

Received 2006 December 12; accepted 2007 January 6

ABSTRACT

We present parameter and abundance data for a sample of 298 nearby giants. The spectroscopic data for this work have a resolution of $R \sim 60,000$, $S/N > 150$, and spectral coverage from 475 to 685 nm. Overall trends in the $Z > 10$ abundances are dominated by Galactic chemical evolution, while the light-element abundances are influenced by stellar evolution, as well as Galactic evolution. We find several super-Li stars in our sample and confirm that Li abundances in the first giant branch are related to mixing depths. Once astration of lithium on the main sequence along with the overall range of main-sequence lithium abundances are taken into account, the lithium abundances of the giants are not dramatically at odds with the predictions of standard stellar evolution. We find the giants to be carbon-diluted in accord with standard stellar evolution and that the carbon and oxygen abundances determined for the local giants are consistent with those found in local field dwarfs. We find that there is evidence for systematic carbon variations in the red giant clump in the sense that the blue side of the clump is carbon-poor (more diluted) than the red side.

Key words: solar neighborhood — stars: abundances — stars: late-type

Online material: color figures, machine-readable tables

1. INTRODUCTION

This paper and its predecessors (Heiter & Luck 2003; Luck & Heiter 2005, 2006) are parts of the former NSF/NASA Nearby Stars Project. In this context, our specific aim is to examine the overall abundance properties of the local region to determine the standard of normalcy (at least in terms of abundances). We wish to do this on a very local scale—15 pc—to examine in detail the abundance distribution. On a larger scale—out to 100 pc—we wish to sample statistically the volume using as probes both solar-type dwarfs and K giants. The primary goal is an increased understanding of the local region about the Sun. We seek the mean metallicity of the region. Using the metallicity data, we want to determine if there are any believable temporal, spatial, or stellar characteristic-related variations in the metallicity. If one considers the local region as a typical volume, then these results can be applied to other locations, and thus will increase our understanding of Galactic evolution. In this paper we consider a volume-selected sample of primarily G/K giants.

Our goal is to sample the G/K giants of the local region out to about 100 pc from the Sun in all directions. We use the *Hipparcos* catalog (Perryman et al. 1997) as our source and sample the region by using cubes 25 pc on a side stacked in the volume with the origin at the solar position. Any cube whose center is within 100 pc of the Sun is considered part of the sample volume. This means the outermost cubes extend to about 113 pc from the Sun. In each cube we select a representative G/K giant, preferring those that have spectral types around K0 III. If such a star is not available, we choose a star with the proper absolute magnitude and color (as computed from the *Hipparcos* data using those stars with spectral types). As a last alternative, we select an earlier type giant (based on spectral type) in the volume (12 stars). In the appropriate volume (radius of 115 pc) *Hipparcos* has about 1550 stars with colors and absolute magnitudes consistent with a G/K

giant. Limiting the sample to stars north of -30° declination, there are of order 1130 stars. Our sample numbers 286 G/K giants (for a total sample of 298 stars), or about 25% of the total population available. In Table 1,³ we present the sample to be considered here and some basic information about the stars contained.

2. SPECTROSCOPIC MATERIAL

High signal-to-noise ratio spectra were obtained during several observing runs between 1997 and 2005. For all observations we used the Sandiford Cassegrain Echelle Spectrograph (McCarthy et al. 1993) attached to the 2.1 m telescope at McDonald Observatory. The spectra continuously cover a wavelength range from about 484 to 700 nm, with a resolving power of about 60,000. Typical S/N values for the spectra are in excess of 150. Each night we also observed a broad-lined B star to enable cancellation of telluric lines where necessary with a S/N exceeding that of the program stars.

We used IRAF⁴ to perform CCD processing, scattered-light subtraction, and echelle order extraction. For all further reductions a Windows-based graphical package (ASP) developed by R. E. L. was used. This includes Beer's law removal of telluric lines, smoothing with a fast Fourier transform procedure, continuum normalization, and wavelength calibration using template spectra. Finally, equivalent widths (W_λ) were determined using the Gaussian approximation to the line profile. The number of lines measured numbered 495,553 with 224,979 of them retained in the final analysis. Only lines with equivalent widths between 10 and 200 mÅ were used in the analysis.

For lines with multiple measurements (order overlap or multiple exposures), the average fractional differences in W_λ are in general lower than 15% for $10 \text{ mÅ} < W_\lambda < 20 \text{ mÅ}$, lower than 10% for $20 \text{ mÅ} < W_\lambda < 30 \text{ mÅ}$, and lower than 5% for $W_\lambda > 30 \text{ mÅ}$.

¹ Department of Astronomy, Case Western Reserve University, Cleveland, OH 44106-7215, USA; luck@fafnir.astr.cwru.edu.

² Department of Astronomy and Space Physics, Uppsala University, SE-75120 Uppsala, Sweden; ulrike@astro.uu.se.

³ Word, Excel, and HTML versions of all tables are available at <http://bifrost.cwru.edu/nstars/GiantTables/GiantIndex.htm>.

⁴ IRAF is distributed by the National Optical Astronomy Observatory, which is operated by the Association of Universities for Research in Astronomy, Inc., under cooperative agreement with the National Science Foundation.

TABLE 1
PROGRAM STARS

HIC	HD	HR	m_V	M_V	Sp. Type	Parallax (mas)	Distance (pc)	l (deg)	b (deg)	RV (km s ⁻¹)	RV Err. (km s ⁻¹)	Source	SB
343.....	225197	9101	5.78	1.04	K0 III	11.29	88.6	74.7	-74.8	25.9	0.8	L	
379.....	225216	9104	5.69	0.76	K1 III	10.30	97.1	118.4	4.7	-28.4	0.2	F	
729.....	448	22	5.57	0.81	G9 III	11.17	89.5	109.0	-43.5	-20.8	0.2	M	
2926.....	3411	156	6.18	1.12	K2 III	9.75	102.6	118.7	-38.7	0.5	0.2	F	
3031.....	3546	163	4.37	0.80	G8 III	19.34	51.7	119.6	-33.5	-84.6	0.1	M	SB?

NOTES.—Shown are the apparent magnitude m_V , absolute magnitude M_V computed using the parallax-derived distance, spectral type (primary source *Hipparcos*; Perryman et al. 1997), parallax from *Hipparcos*, distance from the parallax, Galactic coordinates (l , b), radial velocity and its error, and source for the radial velocity: (L) this work; (F) Famaey et al. (2005); (M) de Medeiros & Mayor (1999). The last column indicates whether the object is a spectroscopic binary (classification from de Medeiros & Mayor 1999). Table 1 is published in its entirety in the electronic edition of the *Astronomical Journal*. A portion is shown here for guidance regarding its form and content.

Equivalent width data for four of our program giants are available from Gratton & Sneden (1987). Limiting the comparison to lines with equivalent widths less than 300 mÅ, we find 133 common lines. A regression analysis gives

$$EW_{\text{LH}} = 0.778 \pm 1.102 + (1.003 \pm 0.0115)EW_{\text{GS}},$$

with an uncertainty of 7.3 mÅ (EW_{LH} refers to our data, while EW_{GS} refers to the Gratton & Sneden values). Twenty-three of our stars can be found in Luck (1991) or Luck & Challener (1995). Examining only lines retained in the respective analyses, there are 3119 common lines. A regression analysis gives

$$EW_{\text{LH}} = -1.741 \pm 0.270 + (0.926 \pm 0.00309)EW_{\text{OLD}},$$

again with a standard deviation of 7.3 mÅ (EW_{OLD} refers to Luck [1991] and Luck & Challener [1995] collectively). As can be seen, the comparison with Gratton & Sneden is excellent. The comparison with Luck (1991) and Luck & Challener (1995), while not as good, is as expected based on the discussion found in Luck & Challener. The data of Luck and Luck & Challener are based on comparable signal-to-noise ratio but lower resolution data from the coudé feed at Kitt Peak National Observatory. Those data have about 50% of the resolution of the current data, so blending is much more of a problem in the older data. Individual lines show common behavior; that is, measures of the same line in different stars tend to show similar behavior in the older data relative to the new data. In addition, two lines separated by only an angstrom can show very different behavior. One line can be in good agreement between the different sources, while the other can be discrepant. In all cases, the lower resolution data give the larger equivalent widths. This behavior points toward significant blending problems in the older data. As a last point, one must acknowledge that the current data could/will still have blended lines in the measurements. Our Fourier transform smoothing of the data points yields characteristic line widths of better than 3 pixels, while the accompanying arcs give slit projections of 2.2–2.4 pixels. This means that the lines are at least marginally resolved, so that additional resolution will not significantly improve the remaining blending problems.

To enable a differential analysis, we obtained a solar flux spectrum using Callisto as the reflector. We used the same spectrograph and reduction procedure as for our program stars. The measured equivalent widths are in reasonable agreement with that determined by other authors from different sources, as shown in Figure 3 of Heiter & Luck (2003).

3. METHODS AND ABUNDANCES

To derive abundances one needs stellar parameters (effective temperature, gravity, and microturbulence), model atmospheres,

and atomic and molecular data. There are two basic approaches to obtaining effective temperatures and gravities. We call the first the “physical” approach. The basic idea is to use photometry to obtain the temperature and then use the absolute magnitude (luminosity) coupled to the effective temperature to derive a mass and thus a gravity. The second approach we label the “spectroscopic” approach. Here one uses the fact that the parameters are imbedded in the spectrum itself. The effective temperature is found by demanding that there be no dependence of total abundance as computed from lines of a single species (Fe I, for example) on excitation potential. Gravity is set by demanding that different ionization stages give the same total abundance. These are known as excitation and ionization balance, respectively. In both cases, the microturbulent velocity is set by demanding that there be no dependence of abundance on line strength. The ideal situation would be that both analyses give the same parameters, but, in general, this is not the case. Here we pursue both approaches. We derive physical parameters, use them as a jump-off point for the derivation of spectroscopic parameters and abundances, and then return to the physical parameters with the same line list as used in the final spectroscopic analysis to derive abundances using the physical parameters.

3.1. Models and Physical Data

To generate abundances for our program stars we have used the new MARCS grid (Gustafsson et al. 2003; see the MARCS Web site). The entire grid (more than 8000 models) has opacity sampling (OS) line blanketing and a wide variety of elemental abundance mixes. For parameters appropriate to G/K giants, these models are two-dimensional (2D). These models require an input mass, and we have selected the $1 M_{\odot}$ subset (which is also the most extensive). For abundances we use CN-processed abundances with overall metallicities spanning -0.5 to $+0.3$ dex in $[M/H]$. We have developed 2D interpolation routines for the grids that return excellent agreement with models of the grid itself. We have also utilized the prior-generation MARCS75 code (Gustafsson et al. 1975). While not a current state-of-the-art model atmosphere generator, this code provides continuity with a wide range of previous analyses, and it has been shown that abundances generated by these models are in good agreement with those generated by other codes. In our discussion, MARCS75 models are those from Gustafsson et al. (1975), while “MARCS” refers to the new models of Gustafsson et al. (2003).

The atomic data for this project have been assembled from a variety of laboratory sources. Bulk sources for oscillator strengths include Fuhr et al. (1988), Martin et al. (1988), and other individual sources too numerous to enumerate. These gf -values are used to determine imputed solar abundances on a per-line basis that are

in turn then used to determine the differential abundances of our program stars. This means that all abundances given here for elements with $Z > 10$ are pure differential abundances with respect to the Sun. While van der Waals line damping is not an especially important parameter in G/K giants, it is in the Sun. We have used the van der Waals coefficients of Barklem et al. (2000) when available and otherwise computed them from the Unsöld approximation (Unsöld 1938). As a point of reference the model used to generate the data for the solar differential analysis was from the new MARCS grid with $T_{\text{eff}} = 5770$ K, $\log g = 4.44$, and $V_t = 0.8$ km s⁻¹ (Grevesse & Sauval 1999). Atomic and molecular data for the syntheses are discussed along with the syntheses themselves.

The line analysis code was that of R. E. L., which derives from the LINES code of Sneden (1973). For the syntheses we have used a variant of the MOOG code of Sneden (1973). The analysis codes have been benchmarked against Kurucz's WIDTH and SYNTE codes, with all codes yielding the same results to within expected numerical accuracy and differences due to assumptions (primarily partition functions and damping). One concern that can be allayed here is the use of a 1D analysis code such as LINES or MOOG with 2D models such as the new MARCS models. This mismatch has been investigated by Heiter & Eriksson (2006), and they conclude that down to gravities of $\log g = 2.0$ there is no problem with the use of a 1D line analysis code coupled to the 2D models.

3.2. Parameters

3.2.1. Physical Parameters

A variety of photometry is available for the program stars. For the effective temperature determination, DDO $C(42-45)$ and $C(45-48)$ (McClure 1976), Geneva $B2 - V1$ (Golay 1972), Johnson $U - V$, $B - V$, $V - K$, and $J - K$ (Mendoza 1963), and Cousins $V - R$ and $V - I$ (Cousins 1976) have been used. All photometry was obtained through the General Catalog of Photometric Data (Mermilliod et al. 1997). Photometric transformations to convert Johnson $V - K$ and $J - K$ to the Johnson-Glass system were taken from Bessell & Brett (1988).

In order to use the photometry in the determination of the effective temperature, the color excess $E(B - V)$ is needed. These stars are generally not located in the Galactic plane, and typical distances are of order 100 pc, so the reddening will be small. Line-of-sight extinctions have been determined using the code of Hakkila et al. (1997) and distances computed from *Hipparcos* parallaxes. These extinctions are essentially determined from (l, b, d) versus A_V relations. However, the extinction within 75 pc of Sun (the Local Bubble) is essentially nil (e.g., Lallement et al. 2003; Breitschwerdt et al. 2000; Sfeir et al. 1999; Leroy 1999; Vergely et al. 1998). This means the distance-derived A_V values will be too large, especially for these very nearby stars. To correct for this, all stars within 75 pc (about 33% of the sample) have had their extinctions (and reddenings) set to zero. For the remaining stars, we have computed the extinction out to 75 pc and subtracted that value from the total line-of-sight extinction. Converting the remaining extinction to $E(B - V)$, we find that 232 of the 298 stars have reddening equivalent to 0.00. There are 51 stars with a reddening of 0.01, 12 have a reddening of 0.02, 1 each at 0.03 and 0.04, and a singular value of 0.23. The last star (HR 6348) is anomalous in that a slight (1°) change in l (or b) can change the reddening to 0.01. Given the uncertainties in the A_V values (typically twice their values) and colors themselves (easily ± 0.01 mag), all of these reddenings are consistent with no reddening, and we proceed assuming that to be the case.

To convert colors to effective temperature we have adopted Bell & Gustafsson (1978) for DDO photometry [$C(42-45)$ and

$C(45-48)$] and for the Geneva system ($B2 - V1$). We have used Houdashelt et al. (2000) for all broadband colors. For stars with $T_{\text{eff}} > 5800$ K we have also used the Künzli et al. (1997) Geneva calibration. Bell & Gustafsson is a rather old calibration, but unfortunately no more recent calibration is available for K giants for the DDO and Geneva photometry systems. There are no differences between DDO and Geneva raw effective temperatures. Nor are there any systematic differences between the various broadband color-derived temperatures [which indicates that our assignment of $E(B - V)$ to 0 in all cases is acceptable]. However, there are systematic differences between temperatures derived from the broadband colors versus the DDO and Geneva colors. We find that the DDO- and Geneva-derived effective temperatures (used as the mean of all individual determinations) can be put on the scale of the broadband photometry by the following transformation: $T_{\text{new}} = 699.4 + 0.876T_{\text{old}}$, where T_{new} is the DDO/Geneva temperature on the scale of the broadband data and T_{old} is the DDO/Geneva effective temperature as given by the Bell & Gustafsson calibration. Our final adopted photometric effective temperature is the simple mean of the various measures. The mean standard deviation of the broadband determinations is 29 K, with an average range of 60 K. We take the uncertainty in the photometric temperatures to be of order 75–100 K. We have compared our adopted photometric effective temperatures to the photometric effective temperatures of Allende Prieto & Lambert (1999) and find a mean difference of 4 K ($\sigma = 80$ K, $n = 212$), in the sense that the temperature in this work is higher. This is a minor difference, and thus, if no photometric temperature is available from our determination, we adopt the Allende Prieto & Lambert value as available.

Having photometric temperatures we next need the gravity for our program stars. We use a procedure much like that of Allende Prieto & Lambert. We enter the isochrones of Bertelli et al. (1994) with our effective temperature, the parallax-derived absolute magnitude (M_V), and their expected uncertainties. From this, we obtain by interpolation the mass and absolute bolometric magnitude. From these the luminosity and gravity follow directly. The process implemented in this manner does not demand the use of a photometric effective temperature; one can use any type of temperature that one wishes. It is possible that no isochrones pass through the allowed temperature and absolute magnitude region. Our routine failed to determine physical parameters for 15 of the 298 program stars. This failure rate is comparable to that of Allende Prieto & Lambert; of the 212 stars in common they were not able to determine masses and gravities for 13 stars. The mean difference in mass (this work minus Allende Prieto & Lambert) is $+0.04 M_\odot$ ($\sigma = 0.27$), and for gravity ($\log g$) the difference is -0.01 ($\sigma = 0.1$). The mean mass of these objects as derived from the photometric temperature is $1.57 M_\odot$, with a standard deviation of $0.41 M_\odot$ and a range of $0.93-3.13 M_\odot$.

The uncertainty in the individual masses can reach nearly 100% based on the confusion level in the isochrones crossing the allowed area in the H-R diagram. A typical value of the mass uncertainty (1σ) is 35%, or about $0.5 M_\odot$. Multiple tracks can traverse the allowed region in temperature and luminosity. Some stars have more than 30 tracks within the allowed region. Our error estimates are consistent with the results of Allende Prieto & Lambert (1999), who show in their Figure 1 surface maps of parameter and mass uncertainties based on their application of essentially the same methods used here.

Another caveat concerning the masses is that in the mass range of interest the evolutionary tracks that the isochrones are based on (Girardi et al. 2000) do not include any mass loss. In addition, the tracks do not follow the evolution beyond thermal

TABLE 2
PARAMETERS AND IRON ABUNDANCES

HIC	HD	HR	SPECTROSCOPIC						MARCS75				PHYSICAL				
			T_{eff}	$\log g$	V_t	[Fe/H]	σ	n	T_{eff}	$\log g$	V_t	[Fe/H]	T_{eff}	$\log g$	V_t	[Fe I/H]	[Fe II/H]
343.....	225197	9101	4818	2.73	1.69	0.20	0.13	350	4844	2.77	1.57	0.24	4651	2.47	1.70	0.12	0.23
379.....	225216	9104	4806	2.67	1.59	-0.02	0.10	355	4857	2.68	1.65	0.00	4715	2.51	1.62	-0.08	-0.03
729.....	448	22	4840	2.83	1.48	0.09	0.10	356	4900	2.85	1.54	0.12	4766	2.49	1.63	-0.02	-0.07
2926.....	3411	156	4657	2.59	1.75	0.31	0.18	334	4755	2.54	1.95	0.33	4476	2.33	1.85	0.21	0.35
3031.....	3546	163	5102	2.80	1.72	-0.56	0.09	262	5126	2.88	1.75	-0.54	5055	2.76	1.71	-0.59	-0.55

NOTES.—Shown are effective temperature T_{eff} in kelvins, logarithmic surface gravity $\log g$ (cm s^{-2}), microturbulent velocity V_t (km s^{-1}), mean and standard deviation of the logarithmic iron abundance [Fe/H] relative to the Sun, number of lines (Fe I) in the determination, mean logarithmic iron abundance as determined from Fe I relative to the Sun, and mean logarithmic iron abundance as determined from Fe II relative to the Sun. Table 2 is published in its entirety in the electronic edition of the *Astronomical Journal*. A portion is shown here for guidance regarding its form and content.

pulsing and into the regime of the second giant branch. This means that the correspondence between the stellar position in the H-R diagram and the isochrones is limited to the first giant branch and helium core-burning phases, with no allowance for mass loss or subsequent evolution. Thus, a lower mass, more evolved star at a fixed temperature and luminosity will be assigned a larger mass, and hence a higher gravity. While possible, this scenario will not affect the majority of the stars, as post-helium burning evolution in the region of the red giant clump is very fast relative to previous phases.

3.2.2. Spectroscopic Parameters

Spectroscopic parameters were derived by enforcing traditional spectroscopic criteria for effective temperature, gravity, and microturbulence. Lines of Fe I were forced to yield zero slope in the relations between total iron abundance and excitation potential by manipulating the model effective temperature. Simultaneously, the total abundances of iron as predicted from Fe I and Fe II were forced into equality using the model gravities. Along with the previous two forcing operations, the slope of the Fe I abundance versus equivalent width relation was minimized, with a target of zero slope.

One of the problems in the overall spectroscopic approach is line selection. It would be preferable that each star be analyzed using exactly the same line list. To work toward this goal, we adopted a two-step procedure. To ensure consistency to the extent possible in the line list a subset of about 70 stars in the dominant temperature regime (4500–5000 K) was used in a preliminary analysis for all elements to be considered. The initial stellar model atmosphere used for this was determined using the physical parameters. These stars were treated on an individual basis to identify and remove discrepant lines. The editing was done by an interactive process which allows one to check for nonlinear trends in the data, determine if there are untoward trends in items such as abundance versus wavelength (indicative of a continuum problem if present), and check how elimination of lines in one relation (such as abundance versus excitation potential) affects another (abundance versus equivalent width). These data were then used to determine the line list to be used in the final analysis: to be retained as a “good” line, a line had to be retained in at least 67% of the stars in the preliminary analysis. The dominant number of retained lines appeared in 90% or more of the stars of the subset considered. This procedure was used for all species *not* examined by detailed spectrum synthesis; i.e., lithium, carbon, nitrogen, and oxygen were *not* treated in this manner. A caveat to the line list must be stated: our selection procedure yields a consistent set of lines for analysis but does not ensure that each line is actually present in each star; it only guarantees that no other lines than

these will be considered. Shifting parameters and vagaries in the observational data can remove lines from consideration, but none can be added. In the second phase of the analysis where final abundances are derived, no further editing of the line data is allowed.

To determine our final spectroscopic parameters the Fe I and Fe II line data were used with a 3×3 grid of models bracketing the anticipated stellar parameters. Three microturbulences were used at each grid point, spanning the range of appropriate microturbulent velocities. These data were then interpolated to determine the stellar parameters where simultaneously there is no dependence of total abundance on lower excitation potential or equivalent width (Fe I only) and the total abundances of iron as determined from Fe I and Fe II are equal. A model with those parameters was then interpolated from the subgrid with metallicity nearest that of the program star. This model was then rerun with the appropriate microturbulence to check the various relations. If necessary, this process was iterated until a self-consistent solution was found.

The internal uncertainty in the spectroscopically determined effective temperature is of order ± 0.005 in terms of $\theta = 5040/T$. This is determined from the uncertainty in the abundance versus potential slope. At 5000 K this translates to 25 K. After consideration of the uncertainty due to the line list selection, we feel that the actual uncertainty is more properly set at the 100 K level, and we use that as the uncertainty in all further discussions. For gravities, the uncertainty is determined by consideration of how much difference can be tolerated between the total iron abundance as given by Fe I versus that by Fe II. Allowing a difference no larger than 0.05 dex yields an uncertainty of ± 0.1 in $\log g$. The uncertainty in the microturbulent velocity is estimated to be at the $\pm 0.3 \text{ km s}^{-1}$ level based on the sensitivity of the abundance versus equivalent width relation.

Stellar parameters and iron data for all three analyses (see § 3.2.3) are given in Table 2. Table 3 gives masses, bolometric magnitudes, and luminosities derived in the physical parameter determination, as determined from the spectroscopic parameters by direct inversion of the gravity, and as derived from the spectroscopic temperature in the same manner as used in the physical parameter determination. Statistical information on the masses, magnitudes, and luminosities can be found at the end of Table 3. What is apparent from Table 3 is that the masses derived from the spectroscopic inversion are much larger than those derived using the physical approach. The difference is due to the larger gravities found in the spectroscopic analysis, which demand larger masses. The effect on the mass of using differing temperatures (i.e., photometric versus spectroscopic) in the physical determination is minor. We present the spectroscopic inversion masses primarily

TABLE 3
MASS AND LUMINOSITY ESTIMATES

HIC	HD	HR	M_V	M_V ERR.	PHYSICAL				SPECTROSCOPIC INVERSION				SPECTROSCOPIC T_{eff}			
					Mass	M_{bol}	L_{Sun}	$\log g$	Mass	M_{bol}	L_{Sun}	$\log g$	Mass	M_{bol}	L_{Sun}	$\log g$
343.....	225197	9101	1.04	0.18	1.20	0.61	1.66	2.47	1.77	0.69	1.63	2.73	1.47	0.68	1.63	2.65
379.....	225216	9104	0.76	0.12	1.60	0.34	1.77	2.51	2.04	0.39	1.75	2.67	1.29	0.41	1.74	2.48
729.....	448	22	0.81	0.14	1.40	0.39	1.75	2.49	2.68	0.46	1.72	2.83	1.29	0.45	1.73	2.51
2926.....	3411	156	1.12	0.19	1.06	0.55	1.69	2.33	1.48	0.68	1.64	2.59	1.31	0.68	1.64	2.54
3031.....	3546	163	0.80	0.09	1.79	0.53	1.70	2.76	1.83	0.57	1.68	2.80	1.84	0.57	1.68	2.80

NOTES.—Shown are the absolute Johnson V magnitude M_V and its error as computed from the *Hipparcos* parallax and its associated error, stellar mass in solar masses, bolometric absolute magnitude, logarithm of the stellar luminosity L_{Sun} in solar units, and surface gravity $\log g$ (cm s^{-2}). For the physical data, the mass and bolometric magnitude were derived using the isochrones of Bertelli et al. (1994) interpolated using the absolute V magnitude and photometric temperature. We then derived L_{Sun} and $\log g$ using standard relations. For the spectroscopic inversion, the spectroscopic temperature was used to determine the bolometric correction using Bessel et al. (1998). The mass was then determined using the spectroscopic value for the surface gravity ($\log g$) and the luminosity using the standard relations. For the spectroscopic data the mass and bolometric magnitude were derived using the isochrones of Bertelli et al. (1994) interpolated using the absolute V magnitude and spectroscopic temperature. We then derived L_{Sun} and $\log g$ using standard relations. Table 3 is published in its entirety in the electronic edition of the *Astronomical Journal*. A portion is shown here for guidance regarding its form and content.

as a point of interest. They are not consistent with the ages expected for G/K giants. The ages that the higher spectroscopic masses imply are less than 1 Gyr, which is not consistent with the expected ages of solar region G/K giants. This discrepancy does not necessarily imply that the spectroscopic gravity is incorrect, only that it cannot be used to infer the mass.

3.2.3. Metal ($Z > 10$) Abundances

Abundances of all species were determined using the spectroscopic parameters and microturbulent velocity. The final line list as defined above was then used in two additional analyses. The first is a spectroscopic analysis using the MARCS75 models (Gustafsson et al. 1975). In this case we have performed a complete solution, that is, excitation and ionization rebalance and a new microturbulence determination. The physical parameters were also used to analyze the final line lists using the MARCS models (Gustafsson et al. 2003). For the physical abundances a redetermination of the microturbulent velocity was also done. In all analyses, the line lists per star are identical (and as consistent from star to star as possible), and all abundances are determined using the same atomic data and solar abundances on a per line basis. The final quoted abundances are differential with respect to the Sun. Given the bulk of the abundance data and the variations possible ($[x/H]$ or $[x/Fe]$, where x is a particular element, mean elemental abundances, per species abundances with standard deviation and number of lines), we present only the mean abundances per element in the form $[x/H]$ in Table 4. The mean was computed as the simple mean over all retained lines per element (not species; all ionization stages were included with equal weight per line). Detailed information about the abundances is available on request from R. E. L.

The internal consistency of the abundances can be evaluated from the spread in abundances from individual lines. For Fe I, Table 2 gives the standard deviation and number of lines used in the analysis on a per star basis. The amount of data precludes the presentation of such information for other species, but in Table 5 statistical information on abundance consistency is presented. For each species with an abundance determined from more than one line, we give the mean and modal abundance, the standard deviation of the mean abundance across the sample, the maximum and minimum abundance, and the number of stars in the determination. Also given is the same information for the standard deviations about the individual means, the standard errors, and the number of lines used. That is, each species abundance for each star has a standard deviation (and standard error and number of lines) associated with it. Table 5 presents the mean standard deviation (and standard error and number of lines) across the sample for each species. Note that there is an intrinsic range in abundance in these stars, so that the sample average (and mode) abundance should be interpreted with caution. However, the standard deviation and standard error of a mean individual abundance are a reflection of the internal consistency of the analysis and should, all things being equal, be independent of the metallicity itself, as well as of the stellar parameters. However, not all things are equal in this case, as the standard deviations actually show a dependence on effective temperature (see Fig. 1).

What could be the cause of the behavior of the standard deviations seen in Figure 1? A related and perhaps more important question is: Does this influence the derived temperatures and gravities? If one jumps ahead and looks at Figure 4, one does not see any difference in the temperature offsets between spectroscopic and physical effective temperatures below 4600 K. Other

TABLE 4
AVERAGE ABUNDANCES WITH RESPECT TO H

SOURCE	Na			Mg			Al			Si			S			Ca		
	S	M	P	S	M	P	S	M	P	S	M	P	S	M	P	S	M	P
HR 9101.....	0.39	0.49	0.28	0.28	0.34	0.17	0.36	0.40	0.38	0.07	0.16	-0.08
HR 9104.....	0.14	0.21	0.07	0.07	0.10	0.01	0.12	0.15	0.12	-0.09	-0.05	-0.18
HR 22.....	0.20	0.28	0.14	0.07	0.12	0.02	0.14	0.19	0.09	0.23	0.26	0.17	0.03	0.08	-0.08
HR 156.....	0.52	0.57	0.34	0.40	0.44	0.33	0.41	0.47	0.26	0.50	0.53	0.53	0.14	0.14	-0.10
HR 163.....	-0.49	-0.47	-0.52	-0.24	-0.23	-0.26	-0.36	-0.34	-0.39	-0.30	-0.29	-0.30	-0.43	-0.39	-0.46

NOTES.—(S) Spectroscopic parameters with MARCS models; (M) spectroscopic parameters with MARCS75 models; (P) physical parameters with MARCS models. Table 4 is published in its entirety in the electronic edition of the *Astronomical Journal*. A portion is shown here for guidance regarding its form and content.

TABLE 5
ABUNDANCE UNCERTAINTIES

Species	Mean	Median	σ	Max	Min	N	Species	Mean	Median	σ	Max	Min	N
Na I.....	0.103	0.110	0.199	0.620	-0.550	293	Fe I.....	-0.017	0.000	0.168	0.310	-0.640	298
σ	0.065	0.060	0.033	0.170	0.010	289	σ	0.121	0.100	0.056	0.530	0.060	298
SE.....	0.038	0.035	0.020	0.120	0.006	289	SE.....	0.008	0.005	0.012	0.200	0.003	298
N	3	3	0	4	1	293	N	332	349	54	356	7	298
Al I.....	0.083	0.090	0.166	0.530	-0.570	290	Fe II.....	-0.018	0.000	0.167	0.300	-0.640	298
σ	0.081	0.080	0.041	0.320	0.000	279	σ	0.157	0.120	0.100	0.560	0.020	298
SE.....	0.057	0.057	0.029	0.226	0.000	279	SE.....	0.038	0.030	0.026	0.170	0.011	298
N	2	2	0	3	1	290	N	18	19	3	27	2	298
Si I.....	0.117	0.120	0.166	0.540	-0.440	297	Co I.....	0.076	0.070	0.198	0.590	-0.540	291
σ	0.122	0.110	0.047	0.370	0.050	297	σ	0.167	0.160	0.038	0.420	0.090	290
SE.....	0.022	0.018	0.012	0.113	0.009	297	SE.....	0.029	0.026	0.011	0.159	0.017	290
N	34	36	5	39	2	297	N	36	38	6	38	1	291
Ca I.....	-0.064	-0.050	0.138	0.330	-0.540	297	Ni I.....	0.001	0.010	0.180	0.400	-0.590	294
σ	0.122	0.110	0.055	0.420	0.040	297	σ	0.147	0.120	0.066	0.460	0.070	293
SE.....	0.033	0.027	0.024	0.276	0.010	297	SE.....	0.015	0.012	0.009	0.087	0.007	293
N	16	17	2	23	2	297	N	102	105	14	109	1	294
Sc I.....	-0.216	-0.220	0.165	0.730	-0.790	283	Cu I.....	0.018	0.030	0.216	0.580	-0.820	287
σ	0.148	0.130	0.080	0.820	0.010	275	σ	0.099	0.090	0.079	0.620	0.000	229
SE.....	0.064	0.054	0.039	0.473	0.005	275	SE.....	0.069	0.064	0.056	0.438	0.000	229
N	5	6	2	7	1	283	N	2	2	0	4	1	287
Sc II.....	-0.064	-0.060	0.140	0.390	-0.580	297	Y I.....	-0.342	-0.330	0.199	0.320	-1.120	287
σ	0.121	0.120	0.040	0.460	0.040	295	σ	0.179	0.170	0.085	0.970	0.000	279
SE.....	0.038	0.036	0.021	0.266	0.014	295	SE.....	0.068	0.058	0.046	0.560	0.000	279
N	11	11	2	13	1	297	N	8	8	2	10	1	287
Ti I.....	-0.024	-0.010	0.144	0.330	-0.570	291	Y II.....	0.026	0.050	0.198	0.690	-0.670	294
σ	0.142	0.135	0.034	0.340	0.070	290	σ	0.171	0.170	0.053	0.350	0.010	293
SE.....	0.016	0.015	0.006	0.069	0.011	290	SE.....	0.088	0.087	0.027	0.202	0.007	293
N	80	84	12	86	1	291	N	4	4	1	7	1	294
Ti II.....	0.042	0.040	0.160	0.390	-0.520	292	Zr I.....	-0.573	-0.560	0.175	-0.100	-1.220	265
σ	0.168	0.150	0.062	0.550	0.010	292	σ	0.125	0.140	0.064	0.260	0.000	257
SE.....	0.042	0.037	0.020	0.246	0.007	292	SE.....	0.073	0.081	0.036	0.150	0.000	257
N	16	17	2	18	2	292	N	3	3	0	3	1	265
V I.....	-0.172	-0.190	0.214	0.590	-0.870	282	Ba II.....	-0.070	-0.040	0.218	0.470	-0.880	295
σ	0.236	0.180	0.203	0.980	0.000	273	σ	0.087	0.080	0.043	0.390	0.020	273
SE.....	0.167	0.127	0.144	0.693	0.000	273	SE.....	0.050	0.046	0.026	0.225	0.012	273
N	2	2	0	2	1	282	N	3	3	1	3	1	295
V II.....	-0.003	-0.010	0.192	0.500	-0.490	284	Pr II.....	-0.116	-0.090	0.159	0.290	-0.780	286
σ	0.167	0.160	0.077	0.420	0.010	260	σ	0.137	0.130	0.058	0.440	0.010	274
SE.....	0.087	0.085	0.040	0.233	0.007	260	SE.....	0.072	0.065	0.033	0.311	0.006	274
N	4	4	1	5	1	284	N	4	4	1	4	1	286
Cr I.....	-0.003	0.015	0.189	0.510	-0.660	292	Nd II.....	-0.058	-0.030	0.191	0.380	-0.810	289
σ	0.139	0.120	0.045	0.410	0.080	291	σ	0.202	0.200	0.063	0.490	0.000	288
SE.....	0.020	0.017	0.010	0.124	0.011	291	SE.....	0.078	0.076	0.026	0.245	0.000	288
N	51	54	8	56	1	292	N	7	7	1	7	1	289
Cr II.....	0.082	0.100	0.206	0.480	-0.640	293	Eu II.....	0.051	0.050	0.163	0.520	-0.460	253
σ	0.147	0.140	0.049	0.460	0.020	293	σ	0.181	0.180	0.071	0.390	0.000	232
SE.....	0.051	0.047	0.021	0.191	0.010	293	SE.....	0.128	0.127	0.051	0.276	0.000	232
N	9	9	1	11	2	293	N	2	2	0	2	1	253
Mn I.....	0.091	0.100	0.273	0.700	-0.850	293							
σ	0.131	0.120	0.058	0.590	0.040	291							
SE.....	0.047	0.042	0.029	0.323	0.018	291							
N	8	9	1	9	1	293							

NOTES.—In the mean column, for each species is shown the mean abundance ($[X/H]$), the mean of all the individual standard deviations (σ), the mean of all the individual standard errors (SE), and the mean number of lines used for the determination of the species abundance (N). The median column is in the same sense as the mean column. The σ column is the standard deviation of the mean. The max and min columns show the maximum and minimum values of the individual abundances. The N column shows the number of stars used in the calculation.

trends are continuous (differences in gravities and iron abundances also found in Fig. 4), so we conclude that the larger standard deviations do not influence the parameters but only represent additional scatter. The increase in the scatter is due to two basic factors: (1) blends increase in the giants as the temperature drops below 4600 K, and (2) the solar data are affected

by blends, and the proportions are similar in the Sun and other stars (both dwarfs and giants) down to about 4600 K. At this temperature the ionization balance changes from Fe II–dominant to Fe I–dominant (similar ionization potentials will do the same), and so attribution of lines to particular identities or even species can change.

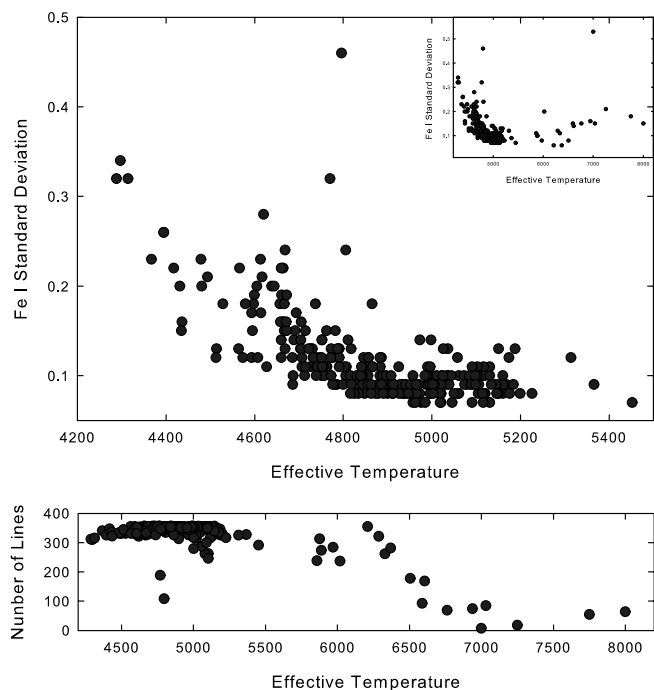


FIG. 1.—Standard deviation of the Fe I abundances as a function of effective temperature. Note the increase in the values with decreasing effective temperature, indicating the increasing prevalence of blends. [See the electronic edition of the *Journal* for a color version of this figure.]

Could better results be obtained by editing the line data for the lower temperature stars on an individual basis? First keep in mind that the number of stars affected is small—only 13 stars have T_{eff} lower than 4500 K out of the sample of 298 stars—so the likelihood of altering overall trends is small. Individual editing has been done for a number of stars, and the result is that one can get somewhat improved consistency (a decrease in the standard deviation from 0.30 to 0.23 is typical), but the trend of standard deviation with temperature remains. There is no systematic difference in the derived effective temperatures. The gravities show some differences, with lower gravities being the norm in individually edited cases. The iron abundances are marginally lower in the cooler stars: a typical difference is -0.08 dex. The upshot is that the parameters and abundances derived here are not significantly impacted by the increase in the line-to-line scatter with decreasing temperature. What will be necessary in going to lower effective temperatures is an alternate bootstrap approach using intermediate “standards.” A new line list will also be needed which uses a cool giant as the source of unblended lines, which are then zero-pointed through the use of the intermediate standard. The selection of unblended lines will be the challenge.

3.2.4. Syntheses

To derive lithium, carbon, nitrogen, and oxygen abundances for our total sample, we have employed spectrum synthesis techniques. Profile matching requires the derivation of either the macroturbulent or the rotation velocity if the lines are resolved. In this sample we find that an additional broadening over the slit profile is needed in all cases. To derive the velocities we use unblended lines in a “sparsely” populated region around 570 nm. The procedure is to compute a grid of model spectra with different broadenings (general usage: Gaussian macroturbulence below 6 km s^{-1} and rotation above that value), with the individual line depths forced to match the observed depth in all cases. The

best-fit velocity is determined from the χ^2 statistics for the synthetic spectra versus the observed spectrum. The velocity data (value and fit type) are given in Table 6 (cols. [7] and [8]). The quality of the fits is evident from Figures 2 and 3. De Medeiros & Mayor (1999) have derived $v \sin i$ values (or limits) for 176 of our program stars using a cross-correlation technique with a focal plane mask (CORAVEL). For the stars where we use a rotation profile, the derived velocities are comparable to those of de Medeiros & Mayor. However, where we use a Gaussian profile (impossible to differentiate from a rotation profile at low velocity in a spectrum synthesis), our velocities are significantly larger than the de Medeiros & Mayor values. This is partially due to our normalization of the Gaussian profile, which increases the macroturbulent velocity by $\sqrt{2}$ relative to a rotation profile. Allowing for the $\sqrt{2}$ normalization factor in our values, a regression analysis for the stars with determined $v \sin i$ values in de Medeiros & Mayor (103 stars) yields

$$v \sin i_{\text{CORAVEL}} = -1.33 + 1.11V_M,$$

where V_M is our derived velocity. This is very like the relation found by de Medeiros & Mayor relative to the $v \sin i$ values of Gray and collaborators (Gray & Nagar 1985; Gray & Toner 1986, 1987; Gray 1989):

$$v \sin i_{\text{CORAVEL}} = -1.15 + 1.18v \sin i_{\text{Gray}}.$$

The Gray values were determined by a Fourier analysis of high-resolution, high signal-to-noise ratio data. It appears that the CORAVEL $v \sin i$ values may suffer from systematic differences with respect to values derived from other techniques.

For the lithium feature we have used all components of ${}^7\text{Li}$ (using the data presented by Andersen et al. 1984) in the 670.7 nm hyperfine doublet to match the observed profiles. These abundances are given in Table 6 (for all three parameter sets), along with a code indicating the quality of fit: A (excellent) to D (poor), while L indicates that the abundance is an upper limit. To demonstrate the quality of the fits and spectroscopic data, we show in Figure 2 three examples of spectrum fits to the lithium feature. Shown in the top two panels are syntheses that vary by ± 0.1 or ± 0.05 from the “best-fit” value. Given the sensitivity of the profile to the lithium abundance, we assign a possible error of $+0.1$ to the upper limits (quality L), ± 0.1 to fits of quality B–D, and ± 0.05 to A-quality fits. We note that a fit to lithium has been done for our solar reflection spectrum using the MARCS model for the Sun. Our synthesis yields a lithium “abundance” for the Sun of $0.89 [\log \varepsilon \text{ where } \log \varepsilon(\text{H}) = 12]$. If one uses a MARCS75 model, the derived Li abundance is 0.85. This is in fair agreement (considering the differences in spectra and models) with the best current value of 1.05 (Asplund et al. 2005a).

To derive carbon abundances we have utilized C I lines at 538.0 and 658.7 nm and Swan system C_2 at 513.5 nm. These lines are of moderate strength, and thus can be synthesized with good precision. For the atomic C I lines we have utilized the oscillator strengths of Biémont et al. (1993). For Swan C_2 we have utilized $f(0, 0) = 0.0303$ (Grevesse et al. 1991) with the relative band f values of Danylewych & Nicholls (1974), along with $D_0 = 6.210 \text{ eV}$ (Grevesse et al. 1991) and theoretical line wavelengths (as needed) from C. Amiot (1982, private communication). We have used these data to determine abundances for each of these features for the Sun from our solar reflection spectrum. For these features we derive $\log \varepsilon(\text{C}) = 8.37, 8.39,$ and 8.50 [with respect to $\log \varepsilon(\text{H}) = 12$], respectively, for 538.0 (C1), 658.7 (C1), and 513.5 (C₂) using a MARCS model and 8.50, 8.54,

TABLE 6
LITHIUM ABUNDANCE DATA

HIC (1)	HD (2)	HR (3)	EFFECTIVE TEMPERATURE			V_M (7)	TYPE (8)	EW (9)	LITHIUM ABUNDANCE			
			T_S (4)	T_M (5)	T_P (6)				S (10)	M (11)	P (12)	Q (13)
343.....	225197	9101	4818	4844	4651	4.45	G	7.1	0.35	0.36	0.12	C
379.....	225216	9104	4806	4857	4715	3.75	G	4.5	0.13	0.17	0.01	D
729.....	448	22	4840	4900	4766	3.75	G	1.7	-0.25	-0.19	-0.34	L
2926.....	3411	156	4657	4755	4476	4.15	G	6.5	0.08	0.20	-0.20	D
3031.....	3546	163	5102	5126	5055	4.50	G	0.3	-0.75	-0.74	-0.81	L

NOTES.—Shown are T_S , T_M , and T_P , the effective temperatures (K) for the spectroscopic, MARCS 75, and physical analysis, respectively; V_M , the macroturbulent or rotational velocity (km s^{-1}) with the type given in the next column: (G) Gaussian macroturbulence, (R) rotation; EW (equivalent width) in mÅ, and lithium EW for the synthesized combined components. Also shown are the abundances $\log \epsilon$, where $\log \epsilon(\text{H}) = 12$; and Q, quality of fit A–D, with A the best fit and L denoting an abundance limit. Table 6 is published in its entirety in the electronic edition of the *Astronomical Journal*. A portion is shown here for guidance regarding its form and content.

and 8.42 for a MARCS75 model. These abundances have been used to zero-point our abundances for the program stars with respect to the Sun for each feature, respectively. Note that the most recent carbon abundance determination for the Sun (Asplund et al. 2005b) yields a mean carbon abundance of 8.39. They adopted

the same gf -values as used here for C I but a different dissociation energy for C₂ (6.297 eV). Since we are interested primarily in differential abundances, the differences for C₂ have little to no effect on our discussion.

In a consideration of carbon abundances in F and G dwarfs, Luck & Heiter (2006) found a significant problem with the abundances derived from the permitted carbon lines. The problem is that with decreasing temperature the permitted lines give increasingly divergent abundances with respect to the C₂ features. The same phenomena occur in these giants. The C I line at 538.0 nm is the most divergent, with the line yielding abundances more than an order of magnitude greater than those from C₂ at 4700 K. The 658.7 nm C I line is better behaved but still shows a divergence. The most likely culprits are unidentified interfering blends. As a result, we have decided to use the permitted C I–derived abundances only at effective temperatures above 6200 K in the G/K giants of this study.

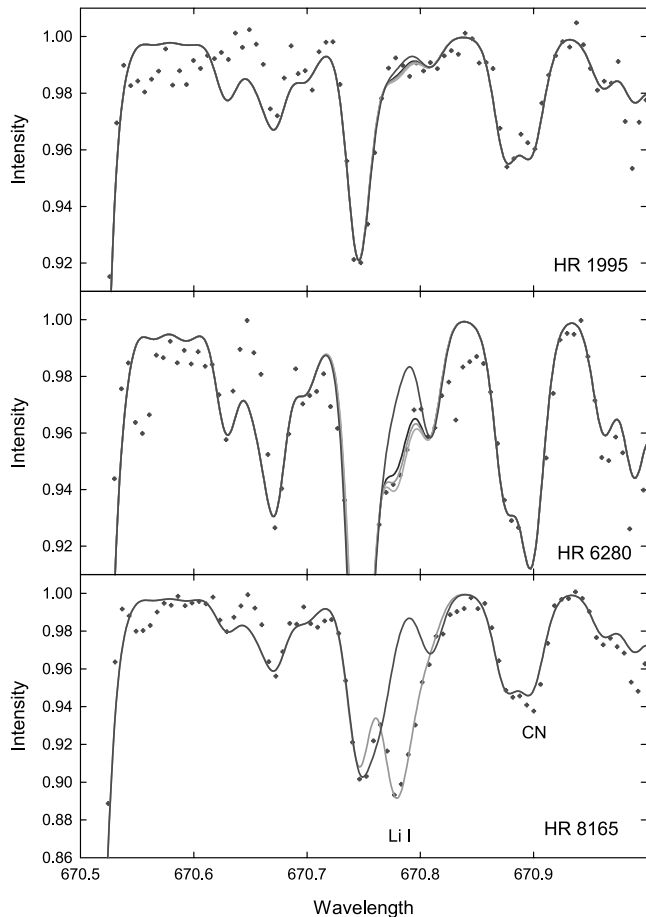


FIG. 2.—Syntheses of the Li I 670.7 nm feature in three program stars. The bottom panel is for HR 8165, which has a moderate-strength lithium line and a high-quality fit. The strength of the Li feature decreases in the other two stars, with the top panel (HR 1995) yielding only an upper limit to the lithium abundance. In the upper two panels the bracketing lines show syntheses at ± 0.1 (top) and ± 0.05 (middle) from the best fit. In each case the dark line is a synthesis without lithium. The effective temperatures (spectroscopic) for the three stars are (top to bottom) 4987, 4710, and 4785 K. Note that there is a CN feature at 670.9 nm. This is one of several CN features used to determine the nitrogen abundance. [See the electronic edition of the *Journal* for a color version of this figure.]

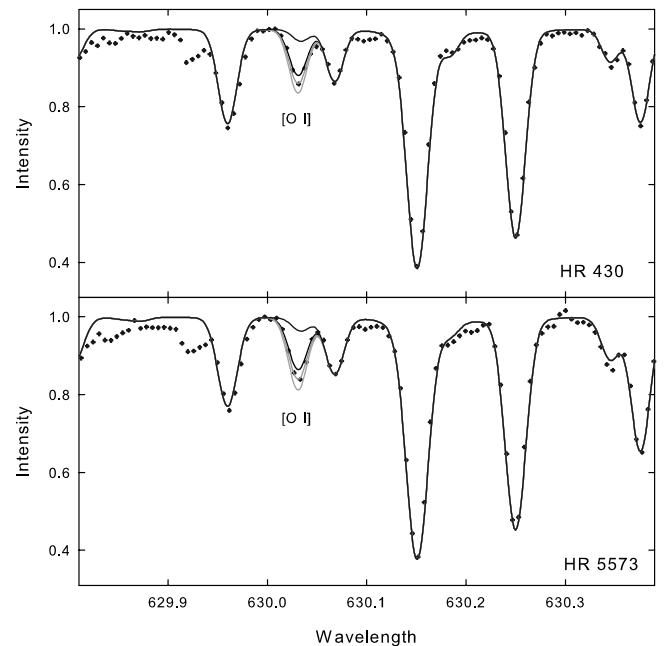


FIG. 3.—[O I] 630.0 nm line in two program stars. The solid dark line synthesis does not include the forbidden oxygen line but does have the blending Ni I line included (at $[\text{Ni}/\text{Fe}] = 0$ in both cases). The effective temperatures of the stars are 5000 K (HR 430) and 4871 K (HR 5573). The best-fitting synthesis in each case is $\log \epsilon(\text{O}) = 8.92$, and the two bracketing syntheses are at nominal oxygen ± 0.1 with respect to the best-fitting value. [See the electronic edition of the *Journal* for a color version of this figure.]

TABLE 7
 CNO DATA FOR GIANTS

HIC	HD	HR	C	N	O	[C/H]	[N/H]	[O/H]	[C/Fe]	[N/Fe]	[O/Fe]	CNO	[CNO/H]	[CNO/Fe]	CN	[CN/H]	[CN/Fe]	C/O
Spectroscopic Analysis																		
343.....	225197	9101	8.55	8.75	9.07	0.05	0.57	0.26	-0.15	0.37	0.06	9.32	0.27	0.07	8.96	0.29	0.09	0.30
379.....	225216	9104	8.30	8.38	8.84	-0.20	0.20	0.03	-0.18	0.22	0.05	9.05	0.01	0.03	8.64	-0.02	0.00	0.29
729.....	448	22	8.36	8.46	8.95	-0.14	0.28	0.14	-0.23	0.19	0.05	9.14	0.10	0.01	8.71	0.04	-0.05	0.26
2926.....	3411	156	8.60	8.77	9.10	0.10	0.59	0.29	-0.21	0.28	-0.02	9.35	0.30	-0.01	9.00	0.33	0.02	0.32
3031.....	3546	163	7.95	7.84	8.77	-0.55	-0.34	-0.04	0.01	0.22	0.52	8.87	-0.17	0.39	8.20	-0.47	0.09	0.15

NOTES.—The C, N, and O columns show the abundance ($\log \varepsilon$) where $\log \varepsilon(\text{H}) = 12$. [C/H], [N/H], and [O/H] are the CNO abundances relative to the Sun using solar CNO determined using a solar reflection spectrum and MARCS and MARCS75 models. For MARCS models, the solar C, N, and O abundances are 8.50, 8.18, and 8.81, respectively, and for MARCS75, the solar C, N, and O abundances are 8.42, 8.16, and 8.75, respectively, except for $T_{\text{eff}} > 6200$, where the C abundance is 8.38 and 8.52 for the two models, respectively. [C/Fe], [N/Fe], and [O/Fe] are the CNO abundances normalized to the Fe content. [C/Fe] = [C/H] - [Fe/H], where [Fe/H] is the iron content of the star relative to the solar value. In the following columns, CNO = $\sum C + N + O$, CN = $\sum C + N$, and C/O = $10^{**}(\text{C} - \text{O})$. Table 7 is published in its entirety in the electronic edition of the *Astronomical Journal*. A portion is shown here for guidance regarding its form and content.

In the determination of the C_2 -based carbon abundance, we have pursued several variations to obtain the best-fit abundance. The first is to match the C_2 feature at 513.5 nm. We then use a grid of carbon abundances about this abundance to examine other C_2 features in the general region. We examine the fits by eye for another estimate, and also do a χ^2 analysis of the syntheses (models) versus the observed data. There is little difference (± 0.05 dex) between the estimates at effective temperatures above 4700 K, but below that temperature the χ^2 approach yields significantly larger carbon abundances. This is because as the temperature decreases the complexity of the spectrum increases, and the number of missing lines in the synthesis also increases. Higher carbon abundances fill in regions using C_2 lines, which yields better χ^2 statistics overall but which make C_2 features in cleaner regions grossly too strong. In these cases we do not use the χ^2 result. Based on this analysis we consider our carbon abundances to be accurate at the ± 0.1 dex level or better.

Oxygen abundance indicators in the available spectral range are rather limited: the $O \text{ I}$ triplet at 615.6 nm and the $[O \text{ I}]$ lines at 630.0 and 636.3 nm. The $O \text{ I}$ lines are problematic due to their extreme weakness in G/K giants, and so we do not consider them further. For the forbidden oxygen lines only 630.0 nm is usable, as 636.3 nm is weak, heavily blended, and complicated by the presence of the Ca I autoionization feature. For our syntheses of 630.0 nm we have used the line data presented by Allende Prieto et al. (2001), except that we have used the experimental oscillator strength for the blending Ni I line (Johansson et al. 2003). In our syntheses we have assumed $[\text{Ni}/\text{Fe}] = 0$. As one would expect, these are not especially difficult syntheses, and this is born out by Figure 3, where we show two typical syntheses. Also shown are bracketing syntheses at ± 0.1 dex from the nominal best-fit abundance. As the bracketing fits are clearly separable from the best fit, we place the uncertainty due to the syntheses in the oxygen abundance at the ± 0.05 level. Our syntheses of the solar $[O \text{ I}]$ 630.0 line gives $\log \varepsilon(\text{O}) = 8.81$ and 8.75, respectively, for the MARCS and MARCS75 models.

Nitrogen abundances were obtained from the CN (6,2) and (7,3) Red system lines in the 671.0 nm region. These determinations were done in conjunction with the Li I syntheses (see Fig. 2, which also shows the CN line at 670.9 nm). Theoretical wavelengths (for both ^{12}CN and ^{13}CN as necessary), lower excitation potentials, and Hönl-London factors were obtained from a program developed by Kotlar (1978). Band oscillator strengths [Red system $f(2, 0) = 9.08 \times 10^{-4}$] and the CN dissociation energy (7.65 eV) were taken from Bauschlicher et al. (1988). This region has been synthesized in the Sun using MARCS and MARCS75

models using the respective C_2 -derived carbon abundance. We find for the Sun nitrogen abundances of 8.18 and 8.16, respectively, for the two models.

In Table 7 we give the CNO data from our various analyses. The carbon and oxygen abundances take into account the interlocking of the abundances primarily through the CO molecule.

4. PARAMETER AND ABUNDANCE COMPARISONS

In this section we discuss the derived parameters and [Fe/H] ratios in terms of the three analyses given here, as well as in relation to previous work. The older studies with which we are primarily concerned are Brown et al. (1989), McWilliam (1990), Luck (1991), and Luck & Challener (1995). In Table 8 we present the mean difference, standard deviation, skew, kurtosis, and number of comparison objects for the various studies. Also presented is a regression analysis for parameters and iron data.

4.1. Internal Comparisons

Within this work there are three analyses, which use either different models or different assumptions in the derivation of stellar parameters. The essence of the differences can be found in Figure 4, where we present effective temperature differences versus spectroscopic temperatures, gravity differences relative to spectroscopic gravities, and [Fe/H] differences relative to spectroscopic [Fe/H] ratios. We wish to emphasize the giants and thus cut off the higher temperatures and gravities in Figure 4. The spectroscopic values are those derived using the MARCS models. In Table 8 one will find the mean differences (computed over all objects) in the sense of MARCS spectroscopic values minus “another” where “another” is either MARCS75 spectroscopic or MARCS physical. We first discuss briefly the differences with respect to the MARCS75 models.

MARCS75 models are 1D models with opacity distribution function line blanketing (precomputed, fixed-abundance, statistical line opacity), whereas the MARCS models are 2D with OS line blanketing (line opacity computed and sampled during model computation). We have used the same lines (and line data) on a per star basis (and overall to the extent possible) to determine spectroscopic parameters for our stars from both types of models. The MARCS75 models yield effective temperatures that are hotter than those of the MARCS models by an average of 50 K. The difference is also dependent on the effective temperature, with higher effective temperatures yielding a somewhat larger difference (see Fig. 4 [top] and the regression given in Table 8). Above 5500 K the two model sets are somewhat closer in derived effective temperature, but at these temperatures there is a tendency for the stars

TABLE 8
PARAMETER AND IRON ABUNDANCE DIFFERENCE AND REGRESSION ANALYSIS

Y	X	$d = Y - X$					$Y = \text{slope} \times X + \text{intercept}$				
		$\langle d \rangle$	σ	Skew	Kurtosis	N	Slope	Error	Intercept	Error	Σ
TS	TO	-49.5	17.0	0.17	1.53	291	0.9834	0.0023	33.2	11.6	15.7
GS	GO	-0.01	0.04	-1.27	3.68	291	1.0161	0.0059	-0.0584	0.0173	0.042
VS	VO	-0.05	0.07	-0.39	6.55	291	0.9036	0.0082	0.1102	0.0145	0.061
FS	FO	-0.02	0.02	-2.19	14.67	291	0.9687	0.0055	-0.0209	0.0009	0.016
TS	TP	97.6	70.6	0.39	5.62	283	0.9747	0.0106	220.0	51.4	70.0
GS	GP	0.26	0.15	-0.34	-0.13	283	1.0076	0.0248	0.2424	0.0654	0.154
VS	VP	-0.06	0.08	0.92	3.79	283	1.0855	0.0131	-0.2101	0.0229	0.078
FS	FP	0.07	0.05	-0.39	1.41	283	1.0502	0.0178	0.0762	0.0031	0.046
TS	TB	152.1	64.9	1.91	6.95	106	0.8609	0.0225	802.0	105.3	55.7
GS	GB	0.25	0.20	0.32	1.16	106	0.8611	0.0584	0.5918	0.1454	0.200
VS	VB	-0.06	0.20	1.60	3.00	106	0.2305	6.7985	1.2380	11.5575	0.197
FS	FB	0.06	0.12	-0.73	0.56	106	0.7502	0.0503	0.0363	0.0113	0.105
TP	TB	49.9	45.2	1.43	5.35	103	1.0003	0.0218	48.5	102.5	45.5
GP	GB	-0.02	0.21	1.27	4.37	103	0.6182	0.0602	0.9316	0.1514	0.179
VP	VB	-0.01	0.14	1.00	2.47	103	0.3323	5.0789	1.0893	8.6341	0.141
FP	FB	-0.01	0.10	-0.42	0.16	103	0.7252	0.0394	-0.0358	0.0089	0.081
TS	TM	142.0	71.9	1.20	3.04	133	0.8523	0.0177	841.2	84.1	58.4
GS	GM	0.00	0.21	0.69	4.37	133	0.9636	0.0570	0.0968	0.1584	0.212
VS	VM	-0.48	0.26	-0.43	7.24	133	0.1479	0.0831	1.3393	0.1785	0.192
FS	FM	0.14	0.06	-0.36	-0.29	133	1.0598	0.0313	0.1491	0.0078	0.061
TP	TM	47.7	53.4	1.37	5.05	129	0.9201	0.0185	426.7	88.0	50.1
GP	GM	-0.31	0.16	1.98	12.37	129	0.8574	0.0504	0.0887	0.1406	0.151
VP	VM	-0.43	0.22	-2.32	14.12	129	0.1561	0.0574	1.3743	0.1236	0.132
FP	FM	0.06	0.05	-0.34	1.03	129	0.9231	0.0253	0.0469	0.0064	0.048

NOTES.—In the first two columns, the first character represents the parameter: (T) temperature, (G) gravity ($\log g$), (V) microturbulence, and (F) [Fe/H]. The second character represents the source: (S) spectroscopic (this work), (O) MARCS75 spectroscopic (this work), (P) physical (this work), (B) Brown et al. (1989), and (M) McWilliam (1990).

to have higher gravities, and thus the MARCS models are from the 1D grid (MARCS 2D models have a maximum gravity of $\log g = 3.5$). The gravity comparison shows that there is little difference in the derived gravities between the two model sets: the mean difference is -0.01 . The same is true for the [Fe/H] comparison: the mean difference is -0.02 . The major difference between the MARCS75 result and the MARCS result is thus the systematic lower effective temperatures derived using the new models. Since photometric temperatures are overall lower than spectroscopic temperatures, the new MARCS models have moved closer to the physical scale relative to the older MARCS75 models.

The summary statement for the MARCS spectroscopic results relative to the physical results is that in the spectroscopic analysis the stars are hotter and have higher gravities and higher abundances. The mean differences are: +98 K for temperature, +0.26 for $\log g$, and +0.07 for [Fe/H]. Inspection of Figure 4 shows that the temperature difference is essentially independent of the effective temperature itself for the physical versus spectroscopic temperatures. Figure 4 (*middle*) shows the difference in spectroscopic and physical gravities as a function of spectroscopic gravity. A cursory inspection shows that the gravity difference in the regime of the 2D models depends on the gravity itself; higher gravities have larger differences. This is a result of the coupling of temperature and gravity in the spectroscopic analysis: as the temperature increases, the gravity must also increase proportionately in order to maintain ionization equilibrium. In Figure 4 (*bottom*) we show the iron abundance differences. For the physical analysis, we have used the total iron abundance as derived from Fe I. The differences show what might be a slight dependence on overall metallicity, but the effect is minor (at most 0.02 dex from [Fe/H] = -0.2 to $+0.1$) and not statistically significant.

One item of further interest at this point is considering the internal consistency of the analysis. This is generally done by looking for trends in abundance versus stellar parameters. In the current data the only “interesting” relation is in [Fe/H] versus effective temperature. Since all three analyses act in a similar fashion, we show in Figure 5 only the data from the spectroscopic analysis. As can be seen, it appears that there might be a dependence of [Fe/H] on temperature. We do not believe this to be the case. First, a formal correlation coefficient determination (Pearson product moment) indicates that there is no correlation over the entire data set. Eliminating those stars with $T > 5500$ K, we still find no statistically meaningful correlation. However, if we eliminate those stars with [Fe/H] < -0.2 along with those having $T > 5500$ K, then there is a correlation in the sense that lower temperatures have higher abundances. However, there is no justification for dividing the data set in this fashion. One could just as easily remove the “metal-poor” stars while retaining all temperatures and determine that there is no correlation (coefficient is -0.00455 with $P = 0.941$) in temperature versus [Fe/H]. The more intriguing aspect of Figure 5 is the gap in the number of stars at temperatures of about 4900 K. The gap is easily seen in the temperature histogram presented in Figure 5 (*top*). It is also present in a histogram of the physical temperatures. If one goes to larger samples of G/K giants (such as those in the Bright Star Catalog or the *Hipparcos* catalog) this dip in the number of stars at 4800–5000 K is not present. One would thus assume that a larger sample would fill the gap with the same dispersion in [Fe/H] as seen in Figure 5, and thus all evidence for a temperature dependence would disappear. As to why this sample is lacking in stars in this temperature range, we can see no reason why our selection technique would necessarily lead to such a

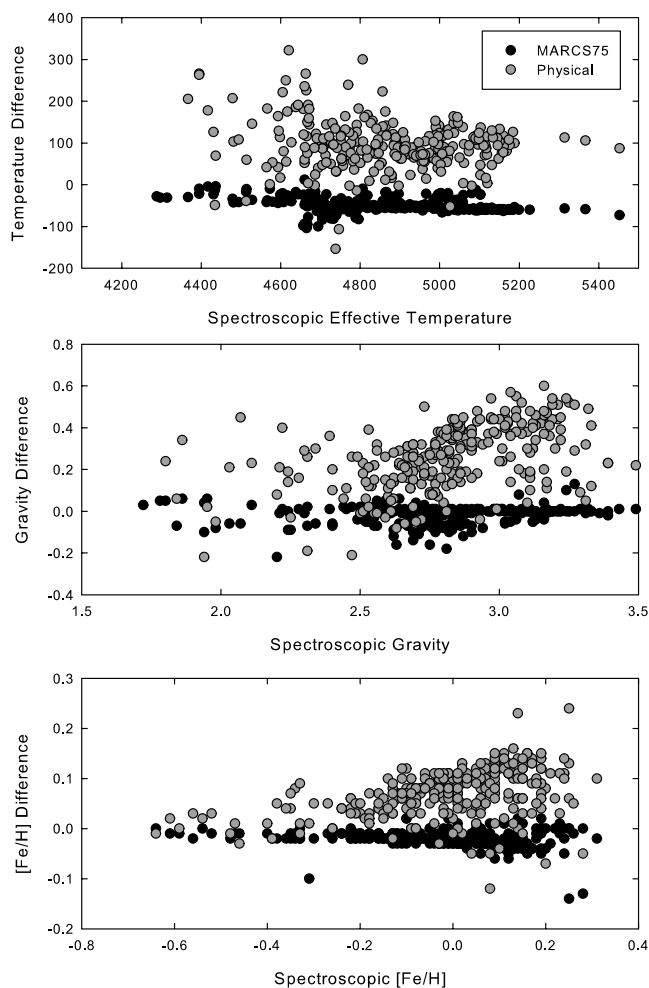


FIG. 4.—Parameter differences (spectroscopic minus physical and MARCS minus MARCS75) vs. spectroscopic parameter for the program stars. See § 4.1 for the discussion. [See the electronic edition of the Journal for a color version of this figure.]

distribution, and thus can only assume it is an unfortunate occurrence.

4.2. External Comparisons

The primary sources for external comparisons are the surveys of Brown et al. (1989) and McWilliam (1990). These studies contain 644 and 671 nearby giants, respectively, of which 106 and 133 are in common with this work. Both studies use stellar parameters derived in a manner consistent with our physical determination. We also briefly mention the studies of Luck (1991) and Luck & Challener (1995), which used combined physical and spectroscopic criteria for parameter determination. We have 12 and 11 stars, respectively, in common with those studies. Statistical data on the comparisons can also be found in Table 8. Da Silva et al. (2006) give a new determination of basic parameters for G/K giants for mainly southern stars, although we have 10 stars in common with their work. As a last item, we briefly consider comparisons with the lithium data of Brown et al. (1989) and Lèbre et al. (2006) and the carbon and oxygen data of Luck (1991) and Luck & Challener (1995).

In Figures 6 and 7 we show the comparison of our parameters with those of Brown et al. and McWilliam, respectively. As expected, the physical temperatures (top panels of both figures) are in “good” agreement, with a common shift of about 49 K in the

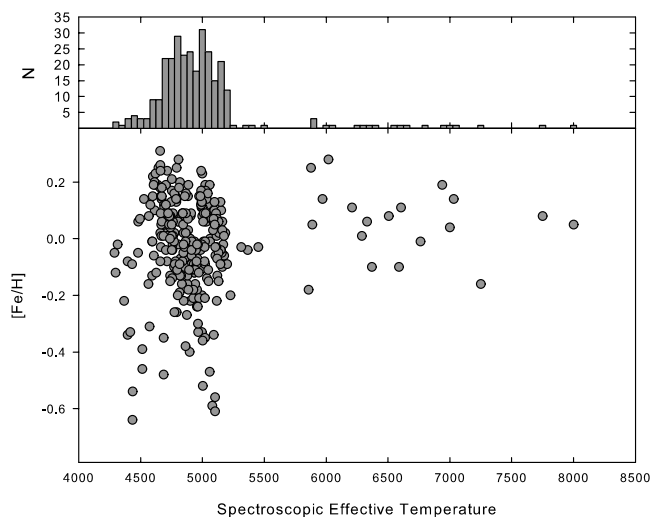


FIG. 5.—Spectroscopic $[\text{Fe}/\text{H}]$ values vs. spectroscopic effective temperature (bottom). There is no statistically meaningful correlation between the quantities. The gap in effective temperatures around 4900 K is real, as demonstrated in the top panel, which shows a histogram of the spectroscopic effective temperatures. [See the electronic edition of the Journal for a color version of this figure.]

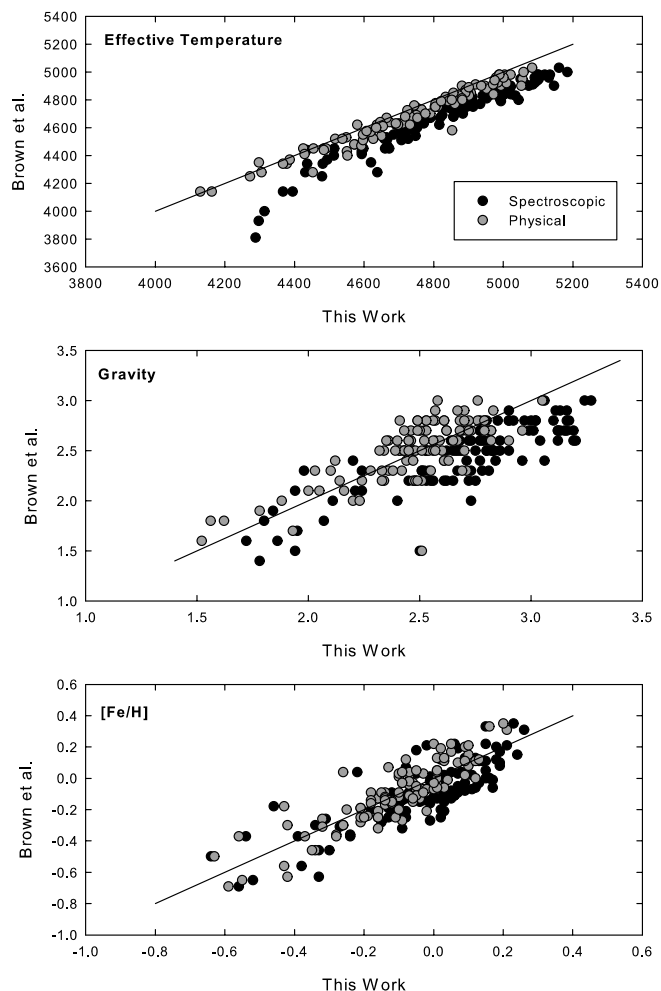


FIG. 6.—Comparison of stellar parameters (effective temperature and gravity) from the current analysis vs. the analysis of Brown et al. (1989). See § 4.2 for the discussion. [See the electronic edition of the Journal for a color version of this figure.]

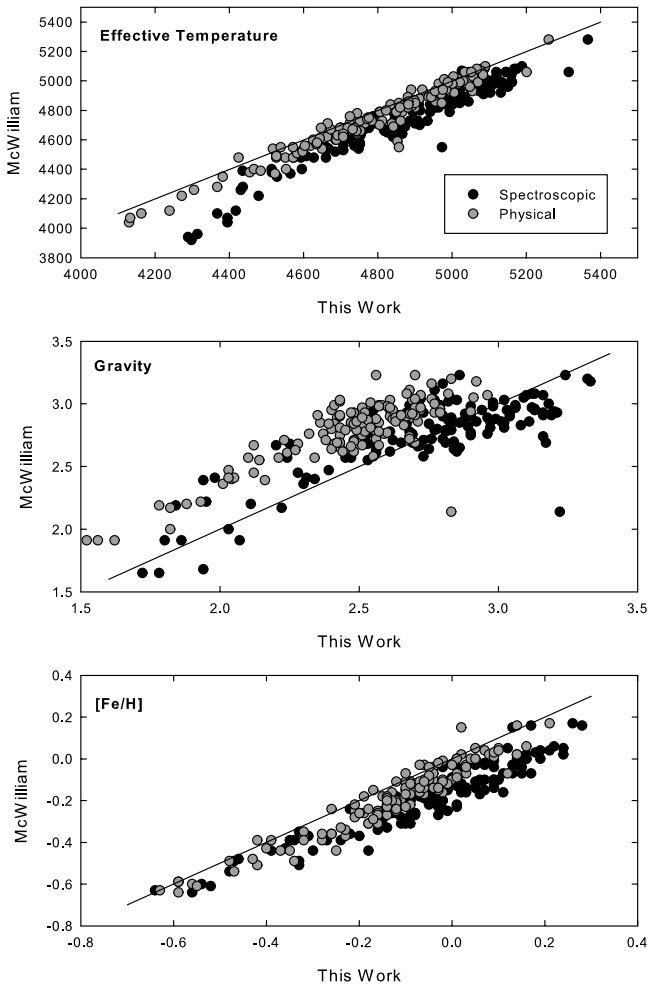


FIG. 7.— Comparison of stellar parameters (effective temperature and gravity) from the current analysis vs. the analysis of McWilliam (1990). See § 4.2 for the discussion. [See the electronic edition of the Journal for a color version of this figure.]

sense that the current physical temperatures are hotter. This difference reflects systematic differences in the photometric calibrations used in the studies: primarily DDO photometry calibrated by Bell & Gustafsson (1978) for Brown et al. and color- T_{eff} fits derived by McWilliam. As indicated in § 3.2.1, the Bell & Gustafsson calibration yields temperatures systematically lower than the Houdashelt et al. (2000) calibration used here.

Gravities used in the various studies are compared in the middle panels of Figures 6 and 7. We find that, as expected, the Brown et al. gravities are in good agreement with the physical values derived here: the mean difference is -0.02 (in $\log g$, with ours being the lower). Our spectroscopic gravities average 0.3 higher in $\log g$ than the Brown et al. values, in excellent agreement with the difference previously noted between our spectroscopic and physical gravities. What is quite unexpected is the difference in the McWilliam gravities and those derived here. The basic methods used to derive physical gravities are the same both in this study and in McWilliam. However, the physical gravity determination of McWilliam is higher by 0.3 in $\log g$ than the values derived here (and by inference, the Brown et al. values). The difference appears to be in the masses used by McWilliam: in McWilliam's Figure 9 the average luminosity in the temperature range $4500\text{--}5000$ K appears to be about $\log(L/L_{\odot}) \sim 1.8$, which leads to masses of about $2.5 M_{\odot}$ from the evolutionary tracks of Sweigart & Gross (1978) and Alcock & Paczyński

(1978) used by McWilliam. This mass is inconsistent with the mass derived here of $1.56 M_{\odot}$, which is based on the Bertelli et al. (1994) isochrones. The tracks that the isochrones are based on (Girardi et al. 2000) are quite different from the older evolutionary tracks used by McWilliam. The McWilliam masses are more consistent with the masses derived by direct inversion of our spectroscopic parameters (see Table 3).

Iron abundance comparisons between the various studies are consistent with expectation. Comparison with the Brown et al. $[\text{Fe}/\text{H}]$ ratios yields a mean difference of 0.06 and -0.01 , respectively, for our spectroscopic and physical determinations. The comparison with the McWilliam values shows a larger difference, which would be expected given the differences in parameters. The differences are $+0.14$ and $+0.06$, respectively, for the spectroscopic and physical parameters of our work. The difference in the physical gravities between the two studies leads to the difference in iron as derived from physical parameters.

The studies of Luck (1991) and Luck & Challener (1995) yield only 12 and 11 objects in common with this study. Both of these earlier studies use photometry to determine effective temperatures and those temperatures are in good agreement with the current physical values once the systematic difference in calibrations noted above is taken into account. Gravities were determined by a physical technique and by forcing ionization equilibrium at the photometric temperature. The results most comparable to ours are thus the pure physical values found in the earlier studies. The physical gravities and iron abundances of Luck (1991) agree well with those found here: the mean differences are 0.01 for $\log g$ and -0.10 for $[\text{Fe}/\text{H}]$. The comparison with Luck & Challener (1995) yields a mean gravity difference of 0.36 but a difference of only 0.04 in $[\text{Fe}/\text{H}]$. The gravity difference is due to the Ca II K line-derived absolute magnitudes used by Luck & Challener being too faint relative to the *Hipparcos* parallax values.

Da Silva et al. (2006) have determined spectroscopic parameters and iron abundances using MARCS75 models for a sample of 72 southern G/K giants. We have 10 objects in common with their study. The mean differences (in the sense of MARCS spectroscopic minus da Silva et al.) are $\Delta T_{\text{eff}} = 80$ K, $\Delta \log g = 0.08$, and $\Delta[\text{Fe}/\text{H}] = -0.07$. Our temperature scale is somewhat hotter than theirs, but overall, the comparison is good.

Brown et al. (1989) derived lithium abundances or limits for 644 giants, of which 106 are in common with this study. For the 37 stars with determined abundances in both studies (and using our physical parameters, as they are closer to those of Brown et al.), the mean difference (this work minus Brown et al.) in lithium abundance is $+0.08$ ($\sigma = 0.15$). A linear regression on the abundances yields $\text{Li}_{\text{US}} = 0.126 + 0.925\text{Li}_{\text{Brown}}$. Examination of the abundance limits shows no unusual discrepancies. Lèbre et al. (2006) have determined Li abundances for 145 bright giants, of which three are common to this study. For two of the common stars the lithium abundances are consistent, while for the third (HR 7449) there is a significant difference in lithium abundance and stellar parameters. For the effective temperature, Lèbre et al. use 4210 K, while our values are 4883 K (spectroscopic) and 4735 K (physical)! The lithium abundance limit derived here for the physical temperature is $+0.05$ [$\log \varepsilon(\text{Li})$, where $\log \varepsilon(\text{H}) = 12$], while Lèbre et al. derive $+0.6$ dex. This implies that at our physical temperature the lithium abundance should be about $+1.2$ dex, which is incompatible with our results. As an aside, Lèbre et al. compare their lithium data to those of Luck & Wepfer (1995) and ascribe any major differences to the imputed use by Luck & Wepfer of incorrect $v \sin i$ values. However, as Luck & Wepfer stated in their paper, they derived macroturbulent velocities from their spectra in the same manner as used here.

Carbon and oxygen data for 23 of the stars of this study can be found in Luck (1991) and Luck & Challener (1995). Parameter differences between the studies make direct comparison difficult, but synthesis equivalent widths are available from all studies for C_2 515.6 nm and [O I] 630.0 nm. Differences in weak line equivalent widths translate directly into abundance differences at the same stellar parameters. The mean difference in the C_2 equivalent width in the sense of this work minus the older studies is -9×10^{-5} nm (-0.9 mÅ), with a mean fractional difference of -10% . This translates into a mean scale difference at the current parameters of about -0.02 dex in the carbon abundance, with a range of about ± 0.15 dex. Remember that the C_2 strength goes as the square of the carbon abundance. For the [O I] line the mean equivalent difference is -1×10^{-4} nm (-1 mÅ), with a mean fractional difference of -8% . These equivalents would yield with our current parameters a scale difference of -0.03 dex, with a range of ± 0.15 dex. Overall, this is rather good agreement.

5. DISCUSSION

It must be admitted here at the start of this discussion that these results more than anything else amplify and to some extent clarify previous results on abundances in local giants. Perhaps the most pressing question is: Which parameter determination yields the correct result? We start with that question, but unfortunately, we have no conclusive answer.

5.1. Which Stellar Parameter Sets Do We Use?

In the best of all possible universes (and actually, in this one), stellar parameters derived from photometry, parallaxes (absolute magnitudes), and isochrone-derived masses should agree with parameters determined from stellar spectra. In this regard, we specifically mean the effective temperature and the gravity. As we have seen, they systematically deviate, with the largest difference being in the gravity. The newer models used here have narrowed the gap between the respective effective temperatures to about 100 K in the G/K giants. This is better than in the past and is due to advances in the photometric calibrations, as well as to the new models being somewhat “cooler” than the previous generation. One can hope that future advances will eliminate the gap. However, closing the temperature gap will not eliminate the problem with the gravities. The difference in gravities (most often expressed as $\log g$) is nearly a factor of 2, and a 100 K change in effective temperature will not erase such a gap. Indeed, inspection of the Fe I and Fe II data for the physical parameters shows that the Fe I minus Fe II difference depends mostly on temperature, with a total range of about 0.4 dex over the temperature range of 4200–5000 K. Modifying the temperature by 100 K will not eliminate this dependence. What will be needed is a fundamental advance in models (3D, hydrodynamic, and non-LTE) and their associated analysis tools to overcome this problem.

The question of which parameter set we use actually comes down to which abundances we believe more. Fortunately (or unfortunately, depending on one’s point of view), the abundances from the two sets are very similar. With a mean difference of 0.07 (spectroscopic being the higher values), there is little to recommend one over the other. The result that tips the balance in the favor of the spectroscopic results in our estimation is the large differences in neutral and ionized abundances noted in the physical results. This difference makes it difficult to interpret/believe abundances determined from ionized species only unless one references the pure ionized abundances to Fe II, but in reality this is little different from using the spectroscopic result in the first place. We prefer the spectroscopic MARCS result in the remainder of

the discussion but refer to the other analyses as needed. As a point of interest, one can find the linear relations between the spectroscopic and physical parameters and [Fe/H] ratios in Table 10.

5.2. Metal ($Z > 10$) Abundances

5.2.1. [Fe/H] Ratios

While Table 4 presents the average abundance per element from all studies, it is difficult from such a listing to obtain a real sense of the data. Metallicity is often interpreted in terms of the [Fe/H] ratio. For this sample we present in Table 9 the [Fe/H] statistics for all three analyses. There is nothing especially surprising about the [Fe/H] ratios; they are consistent with previous analyses (see above) and with the local dwarf abundances of Luck & Heiter (2005, 2006). Since Luck & Heiter used MARCS75 models (and spectroscopic criteria for parameter determination), we use in our comparisons the MARCS75 spectroscopic parameter results for our giants. Note that there is hardly any difference in the spectroscopic MARCS (new models) derived abundances and those derived using the older MARCS75 models. In Figure 8 we show the distribution of [Fe/H] for the local stars versus effective temperature. There is no evidence in this data for significant scale differences in abundance between the giants and dwarfs or for a systematic effect in abundance with temperature. What is apparent is that we have (unintentionally) avoided stars in the temperature range from 5200 to 5400 K for both the dwarfs and the giants. This is largely due to the relative paucity of such stars.

In Figure 9 we present histograms of the dwarf sample broken out in several ways and the histogram of the giant abundances (all derived from MARCS75 models). The top panel shows the subset of dwarfs from Heiter & Luck (2003) that are within 15 pc of the Sun (113 stars), the next panel down shows the total sample (217 stars), followed by the dwarfs excluding all planet hosts (155 stars), and finally the giants (291 stars). It appears that the dwarfs have a more extended high-metallicity tail than do the giants. However, the Luck & Heiter (2006) sample includes a significant number of planet hosts (62). We would estimate the (close-giant) planet host population to be about 7% based on the number of hosts in the 15 pc sample, which means we would expect about 15 hosts in the total dwarf sample. Since planet hosts are metal-rich (Luck & Heiter 2006 and references therein), the total dwarf sample is preferentially metal-rich. However, statistical tests (Mann-Whitney rank sum) show that the differences in the distributions are minimal (except for the 15 pc dwarf sample and the giants, which are statistically marginally different) and could merely reflect sampling uncertainties.

5.2.2. [x/H] and [x/Fe] Ratios

The general way that metal ($Z > 10$) abundances are interpreted is as a function of [Fe/H], in the form of either [x/H] or [x/Fe] versus [Fe/H]. In Figures 10 and 11 we show these relations for all elements, excluding S, Zn, and La, which were determined only in a limited number of stars. The error bars shown in Figure 10 are 1σ error bars from Table 5. Three elements, Mg, Sr, and Ce, are determined from a single line each, and thus have no statistical error bars. In Table 10 we present the statistical information about the metal abundances (both [x/H] and [x/Fe]) along with the regression fits with respect to [Fe/H]. For the most part the data are exactly as expected; the means of the [x/H] ratios are very close to the mean [Fe/H], with the slopes of [x/H] being in the range 0.9–1.1. Among the light α -elements, Si, Ca, and Ti show a modest dependence on [Fe/H], but this is as expected based on previous results; see McWilliam (1997) and Allende

TABLE 9
MEAN [Fe/H] RATIOS

Analysis	$\langle[\text{Fe}/\text{H}]\rangle$	σ	N	Minimum	Maximum
Spectroscopic	-0.017	0.168	298	-0.64	0.31
MARCS75.....	0.003	0.174	291	-0.64	0.42
Physical.....	-0.087	0.156	283	-0.63	0.35

TABLE 10
MEAN SPECTROSCOPIC ABUNDANCE RATIOS AND REGRESSION COEFFICIENTS

ELEMENT	MEAN	σ	N	$[x/\text{H}] = \text{slope} \times [\text{Fe}/\text{H}] + \text{intercept}$					ELEMENT	MEAN	σ
				Slope	Error	Intercept	Error	σ			
[Na/H].....	0.103	0.199	293	1.108	0.024	0.123	0.004	0.068	[Na/Fe]	0.121	0.070
[Mg/H].....	0.087	0.187	250	0.899	0.046	0.096	0.008	0.119	[Mg/Fe]	0.097	0.119
[Al/H].....	0.083	0.166	290	0.887	0.024	0.099	0.004	0.070	[Al/Fe]	0.101	0.073
[Si/H].....	0.117	0.166	297	0.920	0.021	0.133	0.003	0.059	[Si/Fe]	0.134	0.061
[S/H].....	-0.047	0.128	10	0.861	0.351	-0.096	0.038	0.103	[S/Fe]	-0.104	0.098
[Ca/H].....	-0.064	0.138	297	0.725	0.022	-0.052	0.004	0.065	[Ca/Fe]	-0.047	0.079
[Sc/H].....	-0.112	0.141	297	0.702	0.027	-0.099	0.005	0.078	[Sc/Fe]	-0.094	0.092
[Ti/H].....	-0.012	0.144	293	0.820	0.014	0.002	0.002	0.041	[Ti/Fe]	0.005	0.051
[V/H].....	-0.066	0.198	287	1.097	0.031	-0.050	0.005	0.085	[V/Fe]	-0.051	0.087
[Cr/H].....	0.009	0.190	295	1.062	0.022	0.027	0.004	0.064	[Cr/Fe]	0.026	0.064
[Mn/H].....	0.091	0.273	293	1.527	0.032	0.118	0.005	0.092	[Mn/Fe]	0.109	0.128
[Co/H].....	0.076	0.198	291	1.041	0.032	0.095	0.005	0.091	[Co/Fe]	0.094	0.091
[Ni/H].....	0.001	0.180	294	1.037	0.015	0.020	0.002	0.042	[Ni/Fe]	0.020	0.042
[Cu/H].....	0.018	0.216	287	1.015	0.046	0.037	0.008	0.131	[Cu/Fe]	0.037	0.131
[Zn/H].....	-0.007	0.192	6	0.465	1.081	-0.004	0.086	0.210	[Zn/Fe]	0.000	0.193
[Sr/H].....	-0.106	0.202	279	1.196	0.029	-0.095	0.004	0.075	[Sr/Fe]	-0.097	0.081
[Y/H].....	0.026	0.198	294	0.927	0.042	0.042	0.007	0.122	[Y/Fe]	0.044	0.122
[Ba/H].....	-0.069	0.218	295	0.618	0.066	-0.059	0.011	0.192	[Ba/Fe]	-0.053	0.202
[Ce/H].....	-0.023	0.196	285	0.881	0.045	-0.005	0.008	0.127	[Ce/Fe]	-0.003	0.129
[Pr/H].....	-0.116	0.159	286	0.817	0.027	-0.100	0.005	0.078	[Pr/Fe]	-0.096	0.084
[Nd/H].....	-0.058	0.191	289	1.019	0.029	-0.039	0.005	0.082	[Nd/Fe]	-0.039	0.082
[Eu/H].....	0.051	0.163	253	0.828	0.027	0.075	0.005	0.075	[Eu/Fe]	0.080	0.081

NOTES.—The abundance $[x/\text{Fe}] = (\text{slope} - 1) \times [\text{Fe}/\text{H}] + \text{intercept}$, where x is the element and slope and intercept are taken from the linear regression solution for $[x/\text{H}]$ versus $[\text{Fe}/\text{H}]$. The uncertainties are identical.

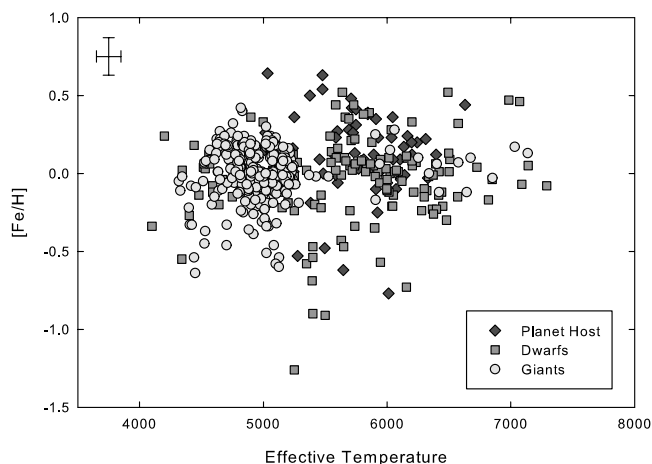


FIG. 8.—[Fe/H] for the giants of this study combined with the local dwarf abundances of Luck & Heiter (2006). Planet hosts have been tagged separately, as they are overrepresented in the dwarf sample. All abundances are computed using MARCS75 models. The distribution of [Fe/H] ratios shows no evidence for substantial differences in scale or dispersion. The error bars shown are ± 0.121 dex for [Fe/H] and ± 100 K for the effective temperature. The [Fe/H] error bar is the mean of the individual standard deviations across the sample (see Table 5). Note that the 95% confidence interval for the individual mean [Fe/H] ratios is of order 0.015 dex, comparable to the symbol size. [See the electronic edition of the Journal for a color version of this figure.]

Prieto et al. (2004) for a thorough discussion of abundance trends in the local neighborhood and Galactic disk and Luck & Heiter (2006) for additional comments. In reaching Cr, we see a few “wild” points, but going onto Mn, Co, and Ni the relations are very tight. There is somewhat more scatter in the elements past Cu, but this is expected, as the abundances here are based on many fewer lines than are the abundances of the iron peak elements (see Table 5).

There are about 11 discrepant points (out of 298) in the Cr data, with both [Cr/H] and [Cr/Fe] showing the same discrepancies. The stars with these discrepant abundances tend to be cooler, and thus have abundances based on a smaller number of lines (10 or less), with the ionized species having large implied abundances that artificially increase the mean abundance. A characteristic of the warmer stars having high Cr abundances is that they have larger than normal microturbulent velocities, indicating there may be problems in the analysis. It must be emphasized that these stars represent only a small fraction of the sample (about 3%), and thus do not substantially influence the overall results.

A curious thing is found in the Mn data: the [Mn/Fe] ratio is a function of the [Fe/H] value (see Fig. 11, *right panels*). The sense is that as [Fe/H] decreases so does [Mn/Fe]. This effect is also seen in the dwarf data of Luck & Heiter (2005, 2006). In Figure 12 we show the combined dwarf and giant data. While there is the possibility of an offset between the studies of about 0.1 dex, it is apparent that both the dwarfs and the giants show the same trend. This trend was first noted by Wallerstein (1962) and Wallerstein et al. (1963) and confirmed by Gratton (1989). The trend is the mirror of that found in the α -elements and most likely implies an origin for Mn in SNe Ia. We note that the adjoining odd elements V and Co show no significant trends with [Fe/H].

The barium data presented in Figures 10 and 11 show several interesting features. The first is the presence of two stars with high barium content. This is most obvious in the [Ba/Fe] data. The star at [Fe/H] = -0.33 , [Ba/Fe] = $+0.71$ is HR 4608, a marginal Ba star (MacConnell et al. 1972). The other star is HR 5487, which is classified as an F2 III star but is more probably a main-

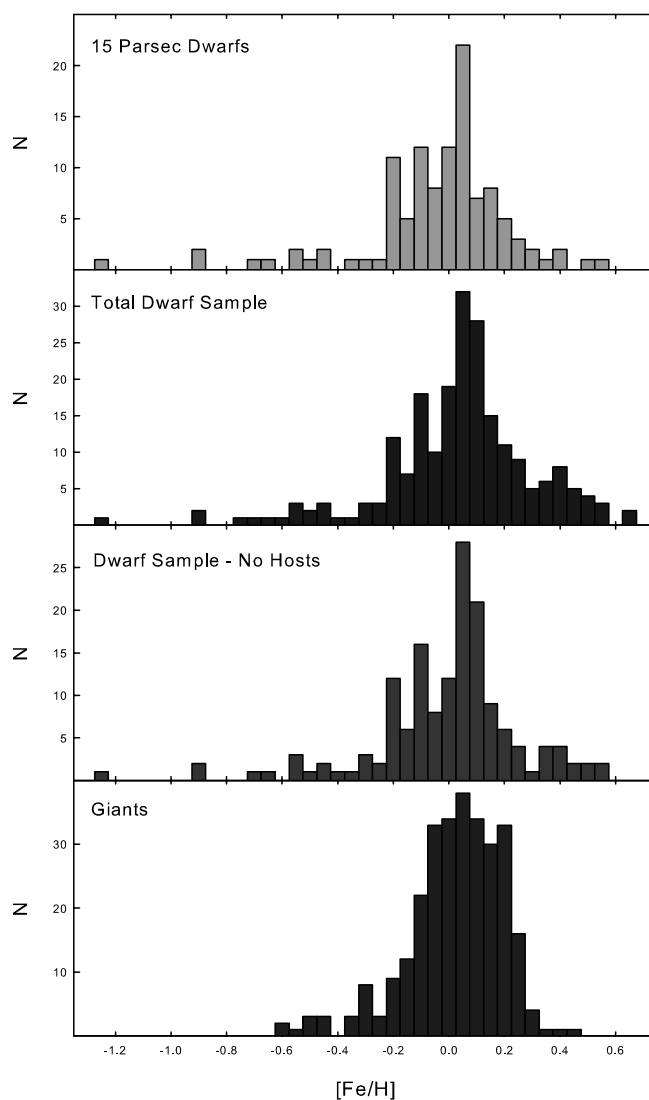


FIG. 9.—[Fe/H] histograms for the 15 pc dwarf subsample of Luck & Heiter (2006), the total dwarf sample, and the giants of this study. It appears that the dwarf samples have a more pronounced high-metallicity tail than do the giants. The mean [Fe/H] ratios are -0.063 , 0.0122 , and 0.003 , respectively. All analyses use MARCS75 models with spectroscopic parameters. [See the electronic edition of the Journal for a color version of this figure.]

sequence star based on mass and gravity. It has never been classified as a Ba star (or a subgiant CH star; Bond 1974). The behavior of the [Ba/Fe] ratios at supersolar [Fe/H] is the distressing feature in the giant barium data. This is seen more clearly in Figure 13, where we show [Ba/Fe] versus [Fe/H] with the dwarf data of Luck & Heiter (2005, 2006) added to the current giant data. The very negative [Ba/Fe] ratios at [Fe/H] of 0.0 to $+0.3$ found in some of the giants are at odds with the dwarf data.

Possible causes for the behavior of the barium abundance include hyperfine structure, non-LTE effects, and microturbulence. Odd numbered nuclei can show hyperfine structure effects, which when allowed for in abundance determinations desaturate the lines and thus lower the derived abundances. The isotopes of Ba are ^{134}Ba , ^{135}Ba , ^{136}Ba , ^{137}Ba , and ^{138}Ba . Solar system estimates for the isotopic ratios are 2.4% : 6.6% : 7.9% : 11.3% : 71.8% (Anders & Grevesse 1989), so one would not expect significant hyperfine effects in these young solar-region objects. This is in accord with the results of Mashonkina & Zhao (2006), who find that significant even nuclei contributions persist in thick-disk

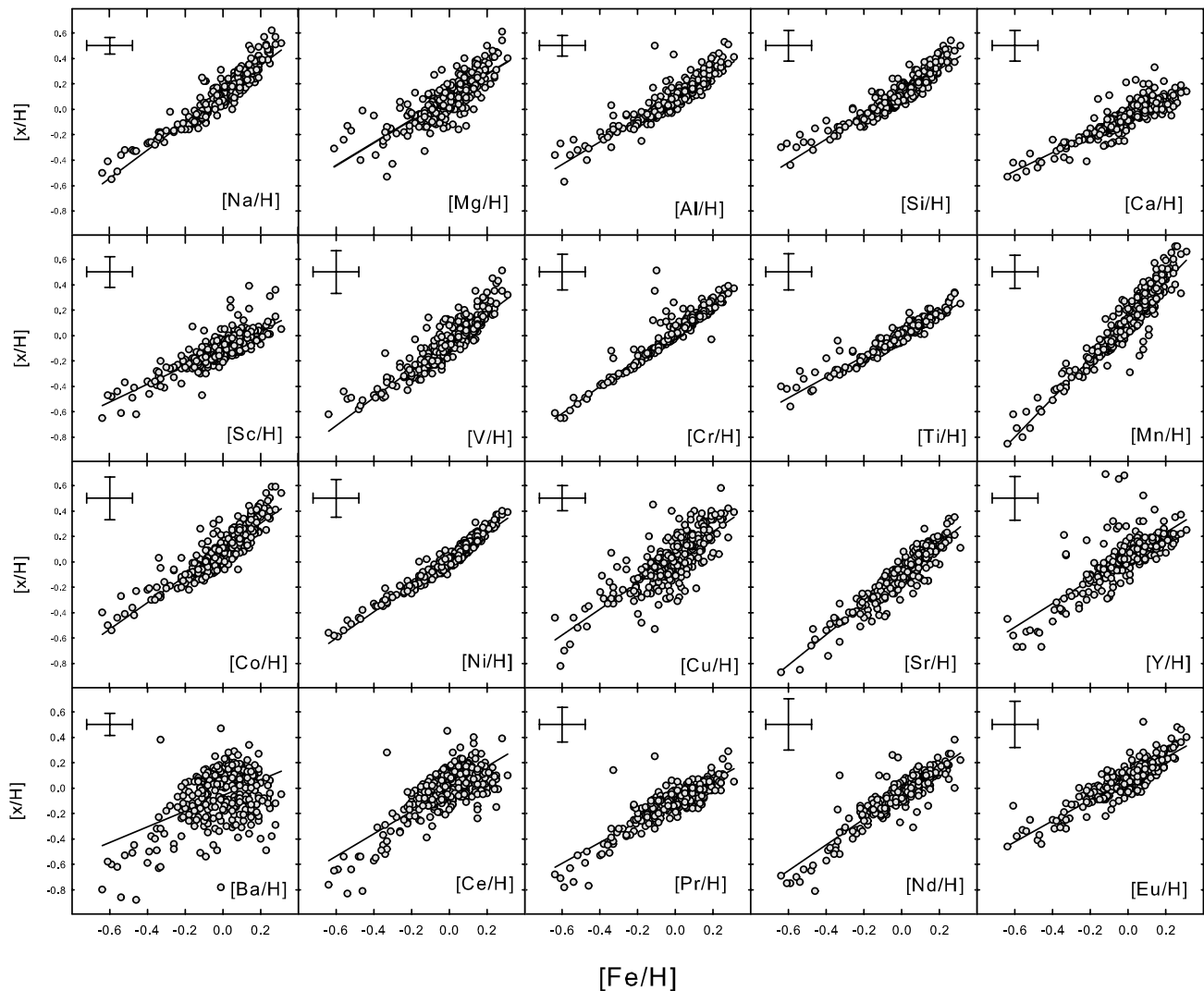


FIG. 10.— $[x/H]$ ratios vs. $[Fe/H]$ for our sample of stars. A linear regression fit is shown. Regression coefficients can be found in Table 10. These ratios are from the spectroscopic analysis using MARCS models. The error bars are the means of the individual standard deviations across the sample (see Table 5). Note that the 95% confidence interval for the individual mean $[Fe/H]$ ratios is of order 0.015 dex, comparable to the symbol size. Mg, Sr, and Ce have no error bars, as the abundances are determined from one line. See § 5.1 for the discussion. [See the electronic edition of the Journal for a color version of this figure.]

stars. In any case, our observed barium abundances are potentially too low, and so hyperfine effects if present would only exacerbate the problem.

While there are no detailed non-LTE calculations for solar-metallicity red giants, the most detailed calculations for metal-poor red giants (Short & Hauschildt 2006) indicate that (1) non-LTE effects become less important with increasing metallicity in the range of $[A/H]$ from -4 to -1 , and (2) the resonance lines are the most affected. The difference in LTE versus non-LTE Ba abundances as derived from the same lines used in this analysis is about -0.03 dex at $[A/H] = -1$ and $+0.03$ at $[A/H] = -4$. The extension of this trend to $[A/H] = 0$, while uncertain, would indicate that non-LTE effects are too small and of the wrong sign to explain the subsolar $[Ba/Fe]$ ratios noted here.

Examination of the giant data shows that the low $[Ba/Fe]$ ratios are associated with somewhat larger than normal microturbulent values, say 2.2 versus 1.6 km s^{-1} . The sensitivity of the Ba Π lines to the microturbulent velocity is such that lowering the microturbulent velocity by 0.5 km s^{-1} will increase the Ba abundance by about 0.4 dex. Such a change would not affect other abundances as severely, as they are based on lines with a mean

equivalent width much less than the $0.012\text{--}0.018 \text{ nm}$ commonly seen in the Ba Π lines. Another potential way to rectify this problem is to invoke a depth-dependent microturbulence. At this point, we merely say that given the current data and techniques, there is no incontrovertible evidence that low $[Ba/Fe]$ ratios exist within the giants of the local region.

Our Eu data are presented in the last panels of Figures 10 ($[Eu/H]$) and 11 ($[Eu/Fe]$). The $[Eu/Fe]$ ratios show an increasing value with decreasing $[Fe/H]$. This is in accord with the local region dwarf data of Woolf et al. (1995). An important indicator of s - versus r -process element formation is the ratio $[Ba/Eu]$. Gratton & Sneden (1994) found that in mildly metal-poor stars this ratio trends downward with decreasing $[Fe/H]$. While our Ba data in giants with $[Fe/H]$ greater than 0.0 are suspect, we see no large-scale problems at lower abundance. We also find that the $[Ba/Eu]$ ratio trends downward as $[Fe/H]$ decreases, in agreement with Gratton & Sneden.

As a last item we consider the ratio $[hs/l_s]$, where $hs = [Nd/Fe]$ and $l_s = [Y/Fe]$. These two elements are used because they have better abundances among the light and heavy s -process elements. The ratio $[hs/l_s]$ is an indicator of neutron exposure (Luck & Bond

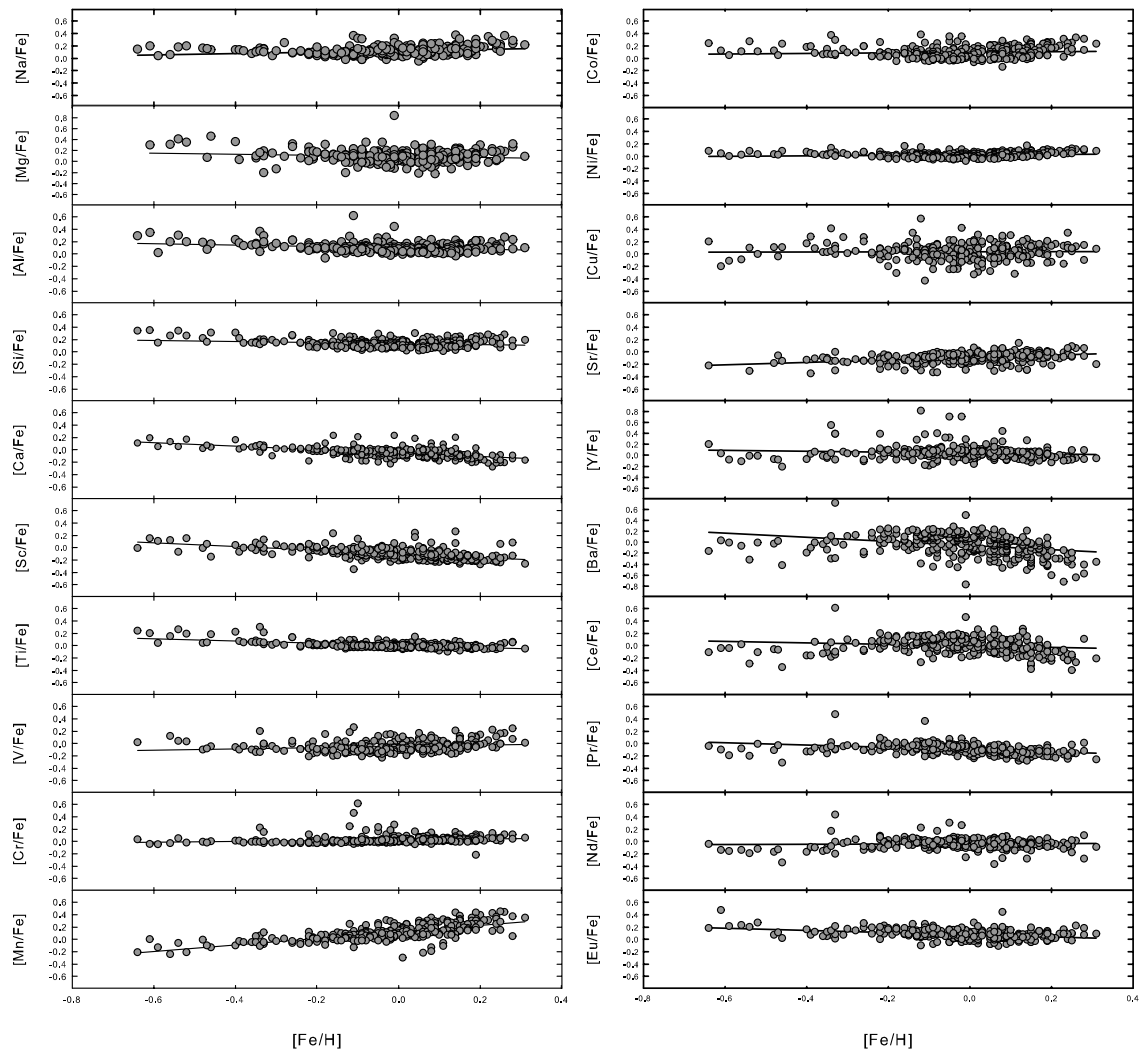


FIG. 11.— $[x/Fe]$ ratios vs. $[Fe/H]$ for our sample of stars. A linear regression fit is shown. These ratios are from the spectroscopic analysis using MARCS models. The error bars (not shown) are comparable to those of Fig. 10. See § 5.1 for the discussion. [See the electronic edition of the Journal for a color version of this figure.]

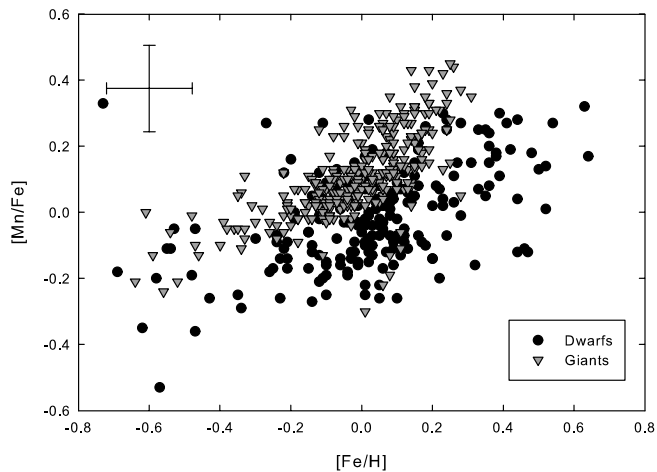


FIG. 12.— $[Mn/Fe]$ vs. $[Fe/H]$ for the giants of this study and the dwarfs of Luck & Heiter (2005, 2006). An offset between the two data sets of 0.1 dex is possible, but both show decreasing $[Mn/Fe]$ with decreasing $[Fe/H]$. This effect was first noted by Wallerstein (1962). Error bars are as in Fig. 10. [See the electronic edition of the Journal for a color version of this figure.]

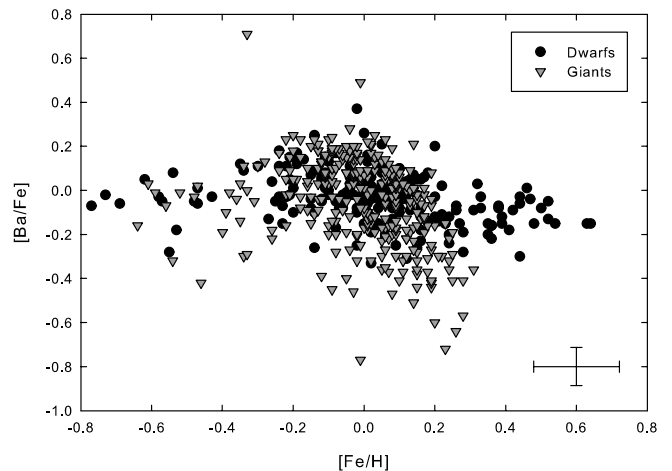


FIG. 13.— $[Ba/Fe]$ vs. $[Fe/H]$ for the giants of this study and the dwarfs of Luck & Heiter (2005, 2006). The lower $[Ba/Fe]$ ratios in the giants with $[Fe/H] > 0.0$ are problematic (see text). Error bars are as in Fig. 10. [See the electronic edition of the Journal for a color version of this figure.]

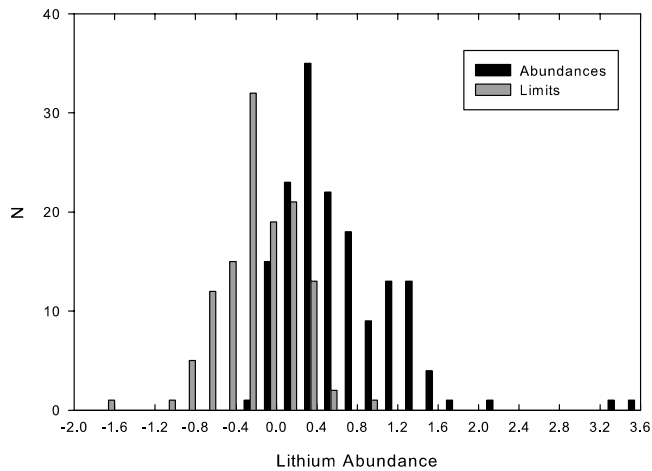


FIG. 14.—Histogram of the lithium abundance data, with the data subdivided between limits and determinations. These data are for the stars with $T_{\text{eff}} < 5500$ K, which effectively removes all dwarfs (F giants by spectral type) in the sample. The two high lithium abundances are the new super-Li stars HR 7820 and HR 8642, both narrow-lined K giants. The dominant number of stars have Li abundances of order 0.5 or less [$\log \varepsilon$ relative to $\log \varepsilon(\text{H}) = 12$]. [See the electronic edition of the *Journal* for a color version of this figure.]

1991). The mean ratio $[hs/l_s]$ in these giants is -0.08 ± 0.05 , which is in good accord with the local region dwarf results of Edvardsson et al. (1993). The interpretation is that the neutron exposure creating s -process elements in the local stars has not changed significantly with the increase in $[\text{Fe}/\text{H}]$ over time.

5.3. Lithium Abundances

Lithium abundances have been determined in a range of local objects, including dwarfs, most recently by Lambert & Reddy (2004) and Luck & Heiter (2006), as well as giants by Brown et al. (1989). Theoretical predictions by Iben (1967a, 1967b) indicate that lithium should be diluted/depleted during the first giant branch by a factor of 60 at $3 M_{\odot}$, decreasing to a factor of 28 at $1 M_{\odot}$. These dilutions/depletions correspond to decreases in abundance of 1.8–1.4 dex relative to the (assumed constant) main-sequence initial value. Therein lies the rub. The surface lithium content of dwarfs is very variable (Lambert & Reddy 2004; Luck & Heiter 2006), spanning up to 2 orders of magnitude at any temperature/mass. While this makes the lithium content of any one star (giant or dwarf) impossible to predict under any evolutionary scheme, one can use overall trends in the data to test the theoretical prediction.

In Figure 14 we show the histogram of lithium abundances separated by detections versus limits. We do not include stars having $T_{\text{eff}} > 5500$ K. The later restriction removes the dozen or so hotter stars, which are nearer (or on) the main sequence (but which were placed in the sample because they have giant luminosity classifications). The stars with determined abundances peak in number at a lithium abundance of about 0.4 dex [relative to $\log \varepsilon(\text{H}) = 12$]. Since the mean mass of these stars is about $1.5 M_{\odot}$, we would expect the main-sequence abundance to be about 1.9 dex for the progenitor objects. This at first appears seriously at odds with the main-sequence data of Lambert & Reddy, which shows that the main-sequence lithium abundance is about 2.6 dex at a mass of $1.5 M_{\odot}$, albeit with a large scatter. The implication is that giants have lithium abundances that are overall lower than what one would expect based on progenitor abundances and standard evolutionary predictions. This is not a new interpretation.

The work of Lambert & Reddy (2004) indicates that the general astration levels of lithium are independent of metallicity

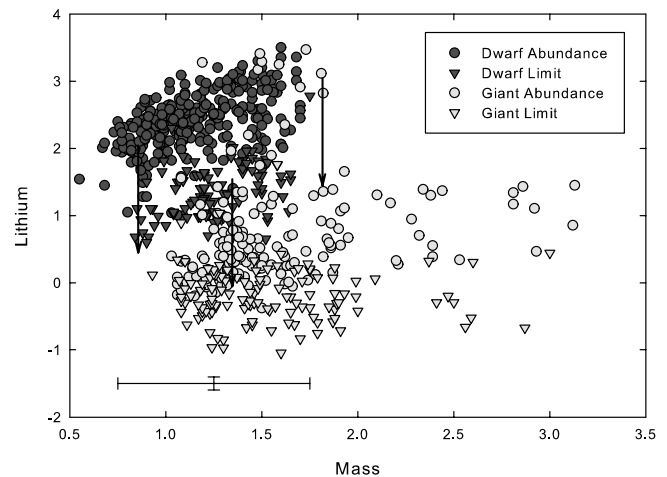


FIG. 15.—Lithium abundance vs. mass. The dwarf data are from Lambert & Reddy (2004). The mass-dependent astration of Li is very apparent. Abundances for giants are from this work and include a few stars more properly considered dwarfs. The downward arrows indicate a dilution factor of 40. Given the astration levels and spread in dwarf lithium abundances, it seems possible that the lithium content in giants is consistent with standard evolution. The error bars are for the giants of this sample. The mass error estimate is $\pm 0.5 M_{\odot}$ (see § 3.2.1), and the lithium uncertainty (± 0.1) is for determined abundances. [See the electronic edition of the *Journal* for a color version of this figure.]

but dependent on mass. In Figure 15 we show their data (lithium versus mass) along with all of the data of this study. Also shown in Figure 15 are indicators of the level of dilution predicted by standard evolution (a representative factor of 40). What is apparent from the figure is that given the scatter in the dwarf lithium abundances and the mass-dependent astration, it is entirely possible that the bulk of the giant lithium abundances are consistent with standard evolution. Since the dilution occurs/starts when the star becomes convective at the base of the first giant branch, the appropriate abundance to use for the dilution can be significantly below the interstellar value of about 3.0–3.2 (determined from the dwarfs themselves; see Lambert & Reddy), which is what has been used in previous interpretations of giant lithium abundances. Some additional dilution may be needed to explain the details of the giant abundances, but it certainly is not at the level one needs if one assumes an initial abundance of 3.0 dex.

Further confounding the interpretation of the giant abundances is that the mean mass of these giants is very close to the mass of the dwarfs in the “Li dip.” The “Li dip” is easily seen in open cluster dwarfs at a mass of about $1.3\text{--}1.4 M_{\odot}$ (Balachandran 1995). However, the “Li dip” is not an especially distinct feature in field dwarfs (Lambert & Reddy 2004; Luck & Heiter 2006). In the open cluster dwarfs lithium is essentially destroyed in that narrow mass ($T \sim 6500$ K) range. It is also true that the mass in which the “Li dip” operates depends on the metallicity; lower metallicity yields lower masses for the dip. Standard evolution operating on a star that experienced the “Li dip” on the main sequence could produce a giant with a very low lithium abundance, provided that the dip mechanism (which is not understood but is probably related to angular momentum transfer) truly destroyed the stellar lithium. The problem with invoking the “Li dip” as the source of the very low lithium abundances is the admixture of lithium abundances, which are observed in the giants (not to mention the dwarfs) at a fixed mass. Another possibility for very low lithium abundances is that these stars are in a more advanced phase of stellar evolution and/or have undergone significant mass loss. As pointed out by Luck (1977), one must be careful with invoking mass loss to account for low lithium

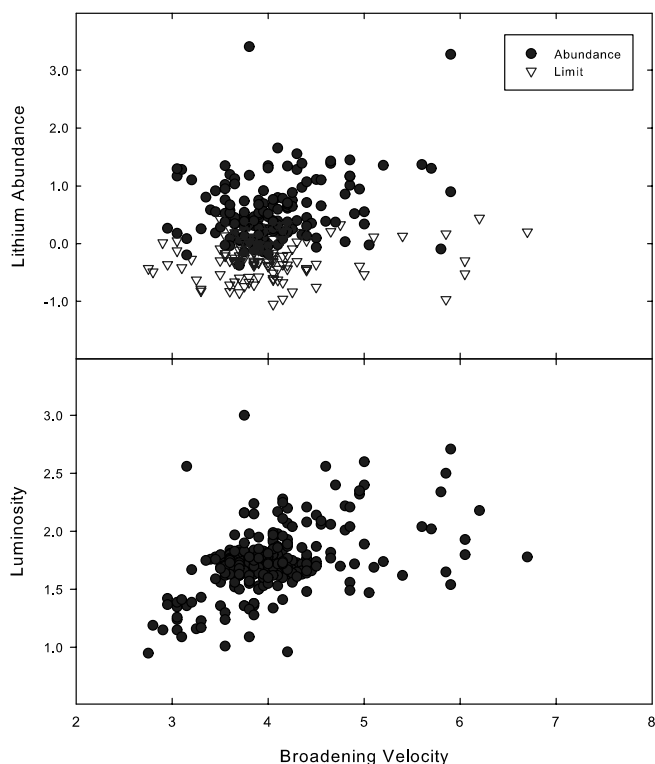


FIG. 16.—Lithium abundance vs. total broadening velocity (macroturbulence/rotation). Here we plot only those stars with $\log g < 3.5$ and $T_{\text{eff}} < 5500$ K, thereby eliminating the few dwarfs in the sample. There is no obvious relation between the velocity and the lithium abundance. The bottom panel shows the correlation between luminosity and the broadening velocity. Note that two higher broadening velocity stars have been left off the plots. They are HR 8703 at [$V_M = 21.8 \text{ km s}^{-1}$, $\log(L/L_\odot) = 1.73$, $\log \varepsilon(\text{Li}) = 1.42$] and HD 116204 at (13.7, 1.29, 0.89). The abundance for HD 116204 is a limit. [See the electronic edition of the Journal for a color version of this figure.]

abundances. Mass loss after envelope homogenization during the first giant branch cannot affect lithium abundances. In fact, in lower mass convective star mass loss will not affect the lithium abundance unless a significant fraction of the star is removed.

Recent work on lithium abundances in bright giants (Lèbre et al. 2006) has claimed that the lithium abundance is a function of the rotation velocity. This extends similar results found in subgiants by Lèbre et al. (1999) and do Nascimento et al. (2000), as well as in giants by de Medeiros et al. (2000) and de Laverny et al. (2003). However, this work finds no such relation in giants (see Fig. 16). The only clear-cut relations seen here are between lithium and temperature and lithium and gravity. The later is evolutionary status; that is, dwarfs versus giants. The broadening velocity does correlate with luminosity (see Fig. 16, bottom). This correlation extends to higher luminosities. We interpret this as meaning that the broadening velocity in the higher luminosity stars is due to macroturbulence and not rotation.

The histogram of giant lithium abundances shows two K giants with very high Li abundances. These stars are HR 7820 and HR 8642, with lithium abundances of 3.41 and 3.28, respectively [relative to $\log \varepsilon(\text{H}) = 12$]. These stars are K giant super-Li stars, that is, K giants with lithium abundances far above the norm for the group. There are about three dozen such stars known (see Charbonnel & Balachandran 2000; Reddy & Lambert 2005). To our knowledge, this is the first report of these stars as super-Li stars. The statistics for super-Li stars is that about 1% of normal K giants are super-Li stars (Charbonnel & Balachandran). There are about 150 stars considered here that are not in the lithium survey

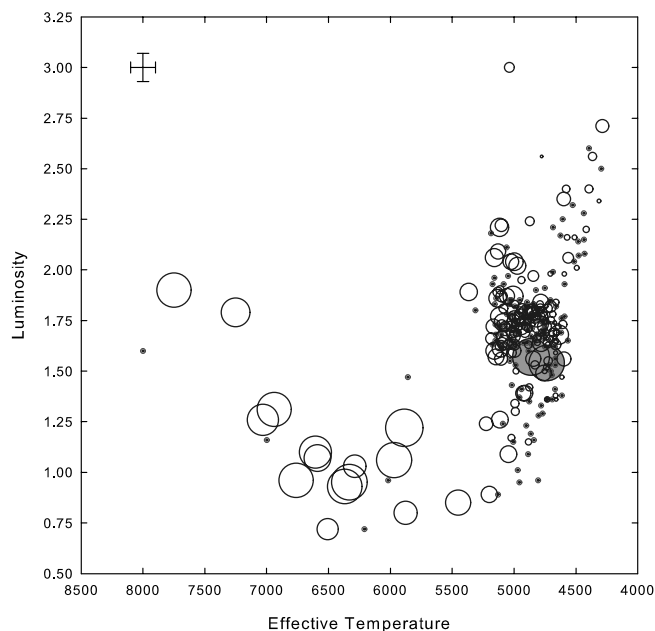


FIG. 17.—H-R diagram for all program stars, with the lithium abundance coded as the size of the circle (radius is proportional to abundance). Limits are coded as circles with dotted centers. The two shaded circles show the super-Li stars found in this work. They correspond to the red giant clump in temperature and luminosity. The error bars assume an uncertainty in effective temperature of ± 100 K. For the luminosity the uncertainty is derived from the uncertainty in the parallaxes and has a mean value across the sample of ± 0.07 in $\log(L/L_\odot)$. [See the electronic edition of the Journal for a color version of this figure.]

of Brown et al. (1989), so our finding of two new super-Li stars is consistent with the previous population estimate. A characteristic of super-Li stars is that they often show larger than normal line broadening (macroturbulence/rotation). HR 8642 does show a somewhat larger than normal macroturbulent or rotational velocity. Super-Li stars are “classified” according to their position in the H-R diagram. In Figure 17 we see that these two stars are at the edge of the red giant clump, the position of one of the two families of such objects (Charbonnel & Balachandran). The best current hypothesis for the clump super-Li stars is due to Charbonnel & Balachandran. The mechanism is an “extra” mixing that occurs at this position in the H-R diagram between the convective envelope and the top of the H-burning shell. The mixing results in the production of ${}^7\text{Li}$, which is then convected to the surface. What is currently missing is a trigger mechanism for the event that can explain the position in the H-R diagram, as well as the tendency toward higher rotation and infrared excesses and the lithium abundances.

5.4. Carbon and Oxygen Abundances

The abundances of carbon, nitrogen, and oxygen in K giants will reflect the effects of both Galactic chemical evolution and stellar evolution. The effects of both are well known, having been studied numerous times; see McWilliam (1997) and Allende Prieto et al. (2004) for a discussion of Galactic evolution trends and Lambert & Ries (1981) for a discussion of evolutionary effects. While Lambert & Ries is 25 years old, it still summarizes the expectations of stellar evolution. The primary Galactic evolution expectation is that the [O/Fe] (and C/Fe) ratio should rise with decreasing [Fe/H]. Stellar evolution will affect the carbon and nitrogen abundances, as well as the ${}^{12}\text{C}/{}^{13}\text{C}$ ratio. Carbon will be converted to nitrogen, the ${}^{12}\text{C}/{}^{13}\text{C}$ ratio will be lowered by partial CN processing, and the products will then be brought to the surface during the first dredge-up. We have no new data on

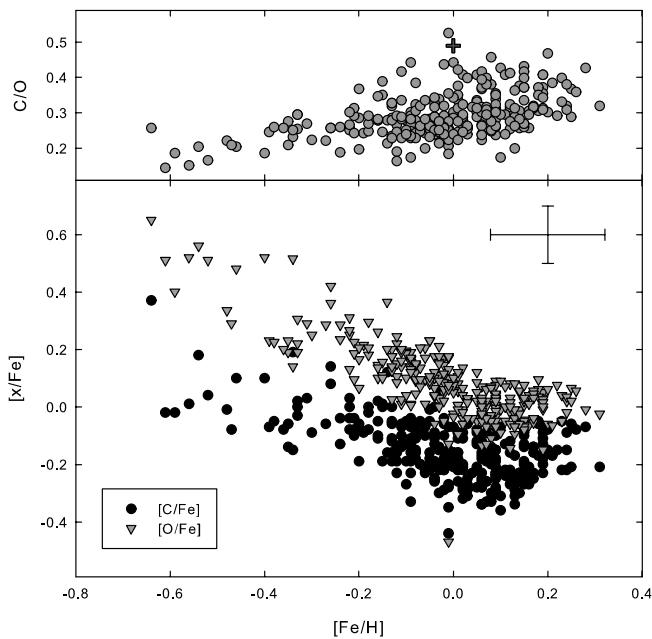


FIG. 18.—*Bottom*: $[C/Fe]$ and $[O/Fe]$ ratios vs. $[Fe/H]$ for the K giants of this study. *Top*: C/O for the giants vs. $[Fe/H]$. The cross in the top panel is the solar C/O ratio as determined from similar data and compatible models (see § 3.2.4). See the text (§ 5.4) for a discussion of these data. The error bars for $[Fe/H]$ are as in Fig. 8, and the uncertainties in the $[C/Fe]$ and $[O/Fe]$ ratios are both assigned a value of ± 0.1 based on the uncertainty in the corresponding ratios relative to hydrogen. [See the electronic edition of the Journal for a color version of this figure.]

the $^{12}C/^{13}C$ ratio in these stars, but previous results (e.g., Lambert & Ries 1981; Luck 1991) indicate that the observed ratios are of order 10–30, which is significantly lower than the presumed initial (solar) ratio of about 90. Our nitrogen abundances derived from CN lines in the lithium region are primarily “placekeepers” which serve to make sure the derived carbon and oxygen abundances are reliable, and so are not discussed further except to note that they are compatible with the discussion that follows.

The relationship between $[Fe/H]$ and $[C/Fe]$, $[O/Fe]$, and C/O is shown in Figure 18. As expected both $[C/Fe]$ and $[O/Fe]$ increase with decreasing $[Fe/H]$. The C/O ratios are subsolar as expected (except for one object, HD 116204) based on the predictions of standard stellar evolution. Carbon is diluted/depleted because of the first dredge-up, while oxygen remains unaffected. Note that the C/O is not independent of $[Fe/H]$ but decreases, implying an enhancement of O relative to C in the more metal-poor stars. Our giant data are in accord with the C/O ratios found using the dwarf data of Luck & Heiter (2006). Their data give solar C/O ratios at solar metallicity, with the C/O ratio declining toward lower $[Fe/H]$ values, albeit with significant scatter. Gustafsson et al. (1999) also found this result in dwarfs. This implies that stellar evolution in this mass and metallicity range yields rather uniform results in the carbon dilution/depletion for the first dredge-up.

In studies of CNO in field giants, the assumption in the past has been that the progenitor abundances are typical of the field dwarfs and that their abundances are similar if not identical to those of the Sun, with a minimum condition of (near) equal ratios of the CNO elements. We are now in a position to check this assumption. In Figure 19 we plot our local giant $[C/Fe]$ and $[O/Fe]$ ratios versus $[Fe/H]$, along with those ratios from the dwarf data of Luck & Heiter (2006). We can see that the dwarf and giant oxygen data overlie each other very nicely; the oxygen abundances of the local dwarfs and giants are equivalent. The carbon data show a

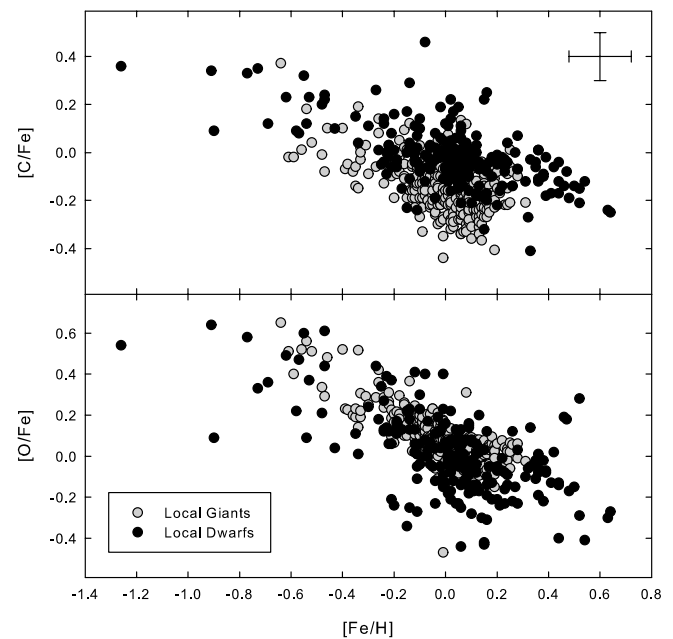


FIG. 19.— $[C/Fe]$ and $[O/Fe]$ data for our giants overplotted with the $[C/Fe]$ and $[O/Fe]$ data for local dwarfs from Luck & Heiter (2006). The oxygen data (*bottom*) show no offset between the dwarfs and giants, while the carbon data (*top*) show a systematic offset of about 0.2 dex (giants having the lower abundance). This is in accord with stellar evolution predictions. Error bars are as in Fig. 17. [See the electronic edition of the Journal for a color version of this figure.]

systematic offset of about 0.2 dex, with the giants having the lower abundances. This is as hoped for and validates our prior assumptions.

There exists the possibility of detecting differences in CNO along the first giant branch as evolution proceeds. The best possibility perhaps is to try to detect differences in red giant branch tip abundances and those in the red giant branch clump. Tautvaišene et al. (2005) attempted this in the open cluster NGC 7789. We show in Figure 20 our $[C/Fe]$ and $[O/Fe]$ data in an H-R diagram. We cannot see any differences in the tip and clump abundances here due to two problems. First, we have an admixture of metallicities that have different $[O/Fe]$ and $[C/Fe]$ ratios as a function of $[Fe/H]$. Second, the tip is undersampled; this survey was not designed to investigate this problem. However, within the $[C/Fe]$ clump data we note an interesting phenomenon: it appears that the blue side of the clump has lower $[C/Fe]$ ratios than the red side. To investigate this further, we made a subset of the data by limiting the luminosities to $1.5 < \log(L/L_{\odot}) < 2.0$ and eliminating the stars in the range $[Fe/H] < -0.3$ (ridding the sample of larger $[C/Fe]$ ratios, which are due to metallicity). We then binned the data in steps of 100 K in temperature, resulting in the data shown in Figure 21. We also show for comparison the $[Fe/H]$ and $[O/Fe]$ ratios, treated in the same manner. What we see in Figure 21 reinforces our finding of a dependence of $[C/Fe]$ on temperature in the clump. Looking at the outermost points, we see that they differ in $[C/Fe]$ by about 0.15 dex, with the blue edge having the higher abundance. While there is a range of $[Fe/H]$ in the data, the $[C/Fe]$ difference cannot be attributed to differing $[C/Fe]$ ratios at different $[Fe/H]$ values. This is because the lower $[C/Fe]$ ratios at $T \sim 5100$ K have mean $[Fe/H]$ ratios of about 0.0, and the cooler stars at the red edge have slightly higher mean $[Fe/H]$ values of +0.1. Since larger $[Fe/H]$ values are associated with smaller $[C/Fe]$ values, the observed trend goes in the opposite sense as the dependence of $[C/Fe]$ on $[Fe/H]$.

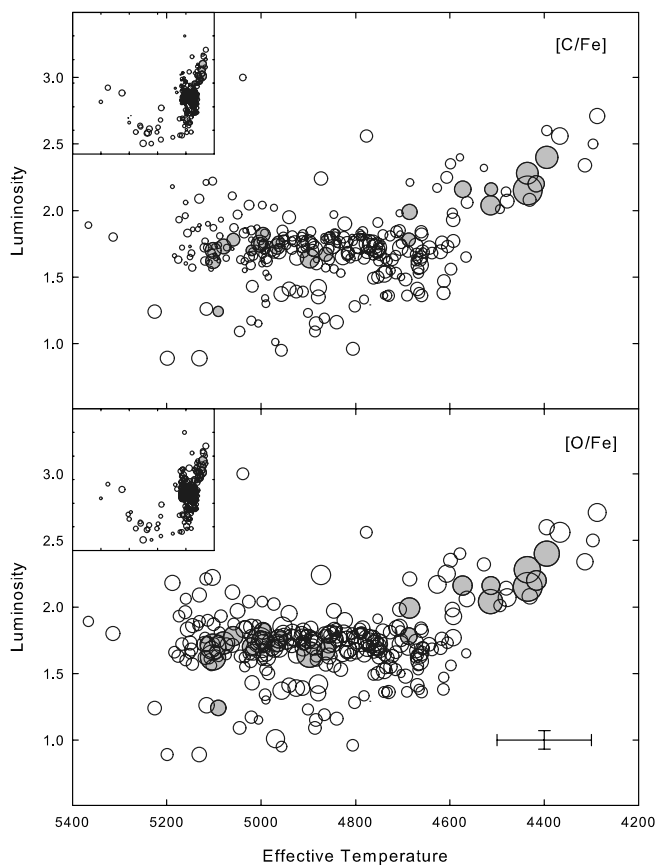


FIG. 20.—H-R diagrams for the $[C/Fe]$ and $[O/Fe]$ data, with the $[x/Fe]$ ratios in each proportional to the bubble radius. The insets show the complete data sets, while the larger figures show the region of the giant branch. Note that the larger circles in the $[O/Fe]$ (and $[C/Fe]$) data indicate more metal-poor stars. The oxygen data are essentially uniform across the H-R diagram, while there appears to be a tendency for smaller $[C/Fe]$ ratios to be clustered toward the blue side of the red giant clump. The shaded circles show stars with $[Fe/H] < -0.3$, which show larger $[C/Fe]$ and $[O/Fe]$ ratios. Error bars are as in Fig. 16. [See the electronic edition of the *Journal* for a color version of this figure.]

If we accept the trend in $[C/Fe]$ at face value, what could be the cause? Abundance trends with temperature make the determiner of abundances uncomfortable in general. Here there exists a second analysis with the same type of models but with different parameters: the physical parameter analysis. That analysis returns the same results as above, with the only difference being that the clump moves in temperature due to the systematic offset of the analyses. Another potential problem is that cooler stars could have systematically higher continua levels that lead to abundance overestimates. Examination of the normalized spectra leads us to believe that nothing systematic exists in the continua placement, and if anything is problematic that perhaps the continua are too low!

Could there be a reason for such a differentiation in $[C/Fe]$ based on stellar evolution? The red side of the clump corresponds to the region where these stars ascend the red giant branch. Stars in that phase, while having begun to mix, have not yet experienced the He flash. The stars toward the blue side of the clump are more likely to be He core-burning and completely mixed. Thus, the difference could be that the abundances on the red side are influenced by incompletely mixed stars, which have not completed dilution of surface carbon, while the blue side is dominated by the completed process, which yields the lower $[C/Fe]$ values. The obstacle to this scenario is the relative times for the ascent and the He core-burning phases. The core burning lasts much longer than the

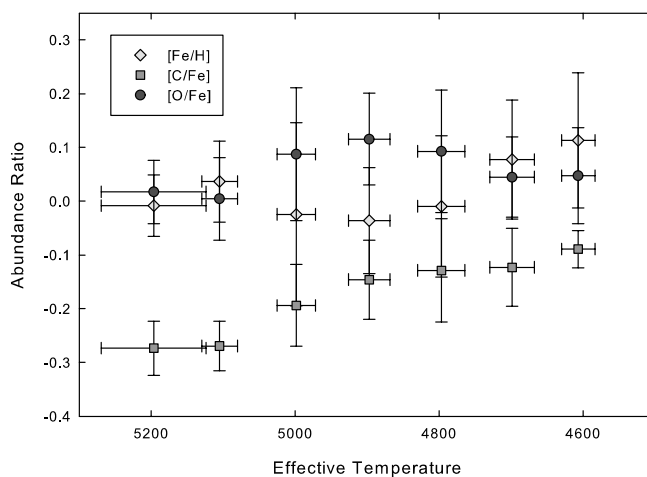


FIG. 21.—Temperature-binned $[C/Fe]$ ratios for clump red giants vs. temperature. Stars with $[Fe/H] < -0.3$ have been removed from the averages. Also shown are $[Fe/H]$ and $[O/Fe]$. Note that $[C/Fe]$ decreases with increasing temperature, while there is no discernible trend in either $[Fe/H]$ or $[O/Fe]$. [See the electronic edition of the *Journal* for a color version of this figure.]

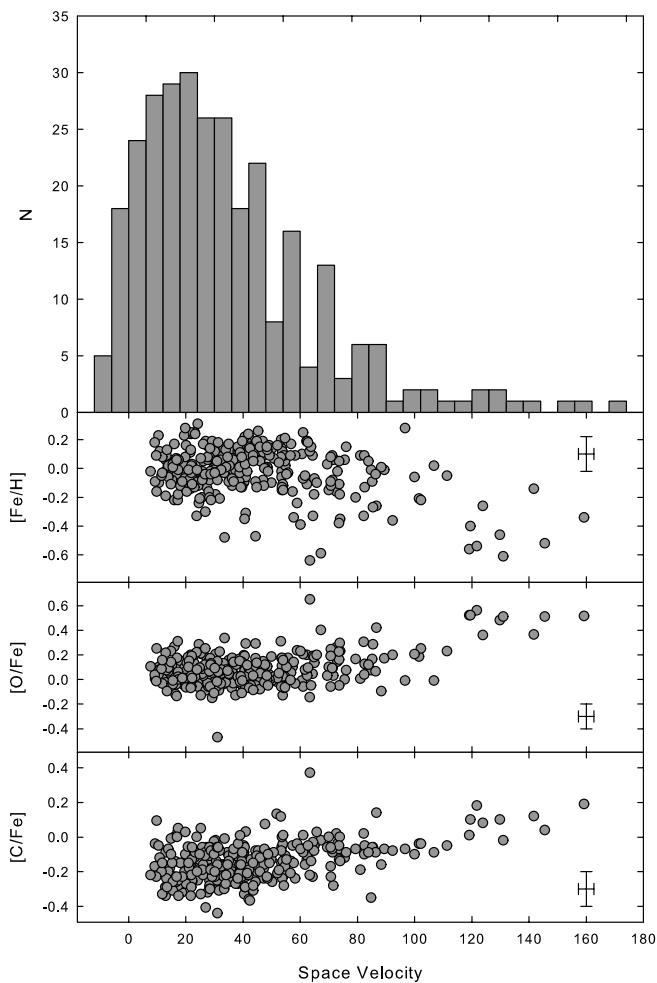


FIG. 22.—Histogram of space velocities for the program stars. It is very akin to that found in larger samples of dwarfs and giants. As expected $[Fe/H]$, $[O/Fe]$, and $[C/Fe]$ all display a dependence on total space velocity. The velocity error shown is the mean of the uncertainty in the total velocities, which is computed as the quadrature sum of the errors in U , V , and W . [See the electronic edition of the *Journal* for a color version of this figure.]

ascent, so the observed number of stars along the red edge of the clump with larger $[C/Fe]$ ratios is much higher than expected. What is needed to further examine this problem is a study of the tip CNO abundances and increased sample size overall to allow more fine-tuning in terms of limiting the $[Fe/H]$ ranges used. The tip will allow the full range of stellar evolution effects to be studied, while the larger sample size will give a better allowance for Galactic chemical evolution effects.

5.5. Kinematics and Abundance

The stars of the local region are dominated by stars of the thin disk population, with some contamination by the thick disk, and possibly by the halo. These populations are usually distinguished by kinematics and metallicity. In Figure 22 (*top*) we show the histogram of total space velocity for our program stars. Space velocities were computed for the sample using the *Hipparcos* proper motions (Perryman et al. 1997) and radial velocities from either de Medeiros & Mayor (1999) or Famaey et al. (2005), or determined from our spectra (accuracy of about ± 1 km s⁻¹ based on comparison with de Medeiros & Mayor and Famaey et al.). We calculated the space velocity from the (U , V , W) components of the motion computed using the formalism given by Allende Prieto et al. (2004).

The mean of the total space velocity distribution is 43.7 km s⁻¹, with a standard deviation of 26.4 km s⁻¹. The mean U -, V -, and W -velocities (heliocentric) are -9.4 , -17.5 , and -9.2 km s⁻¹, respectively. These values are in accord with the values from much larger local samples analyzed by Famaey et al. (2005) (K/M giants) and Nordström et al. (2004) (F dwarfs). The distribution of velocities in this sample parallels those of the larger samples.

In the bottom panels of Figure 22 we plot the $[Fe/H]$, $[O/Fe]$, and $[C/Fe]$ ratios versus total space velocity. As expected, higher

total velocities are associated with lower $[Fe/H]$ values. This implies that higher total velocities should also be associated with larger $[O/Fe]$ and $[C/Fe]$ ratios. This is the case. The exception is that the most metal-poor star in the sample (HR 8852) has a relatively low space velocity (about 60 km s⁻¹). The dominant contribution to the total velocity for HR 8852 is from the W -velocity (about 60 km s⁻¹), which is the component perpendicular to the plane.

6. CONCLUDING REMARKS

In this study we have presented abundance data on 298 stars in the local neighborhood. We find these G/K giants to have overall metallicity levels consistent with the dwarfs in the local region. Lithium abundances in these stars are severely diluted, but once the “initial” dwarf abundances are taken into account the dilution is most likely not substantially in excess of that predicted by standard evolutionary models. The CNO elements have been rearranged due to the first dredge-up, and that process leads to abundances that are consistent with CNO abundances determined from local dwarfs that are then subjected to standard stellar evolution. The most surprising result found in the CNO abundances is the strong indication that $[C/Fe]$ varies systematically from the red edge of the giant clump to the blue edge.

This research was partially funded by NSF grant AST 00-86249. We acknowledge the financial support of Case Western Reserve University that has made it possible to obtain the observations used in this work. Use was made of the SIMBAD database, operated at CDS, Strasbourg, France, and satellite sites, and of NASA’s Astrophysics Data System Bibliographic Services.

REFERENCES

- Alcock, C., & Paczyński, B. 1978, *ApJ*, 223, 244
 Allende Prieto, C., Barklem, P. S., Lambert, D. L., & Cunha, K. 2004, *A&A*, 420, 183
 Allende Prieto, C., & Lambert, D. L. 1999, *A&A*, 352, 555
 Allende Prieto, C., Lambert, D. L., & Asplund, M. 2001, *ApJ*, 556, L63
 Anders, E., & Grevesse, N. 1989, *Geochim. Cosmochim. Acta*, 53, 197
 Andersen, J., Gustafsson, B., & Lambert, D. L. 1984, *A&A*, 136, 65
 Asplund, M., Grevesse, N., & Sauval, A. J. 2005a, in *ASP Conf. Ser.* 336, *Cosmic Abundances as Records of Stellar Evolution and Nucleosynthesis*, ed. Thomas G. Barnes III & Frank N. Bash (San Francisco: ASP), 25
 Asplund, M., Grevesse, N., Sauval, A. J., Allende Prieto, C., & Blomme, R. 2005b, *A&A*, 431, 693
 Balachandran, S. 1995, *ApJ*, 446, 203
 Barklem, P. S., Piskunov, N., & O’Mara, B. J. 2000, *A&AS*, 142, 467
 Bauschlicher, C. W., Langhoff, S. R., & Taylor, P. R. 1988, *ApJ*, 332, 531
 Bell, R. A., & Gustafsson, B. 1978, *A&AS*, 34, 229
 Bertelli, G., Bressan, A., Chiosi, C., Fagotto, F., & Nasi, E. 1994, *A&AS*, 106, 275
 Bessell, M. S., & Brett, J. M. 1988, *PASP*, 100, 1134
 Bessell, M. S., Castelli, F., & Plez, B. 1998, *A&A*, 333, 231
 Biémont, E., Hibbert, A., Godefroid, M., & Vaecck, N. 1993, *ApJ*, 412, 431
 Bond, H. E. 1974, *ApJ*, 194, 95
 Breitschwerdt, D., Freyberg, M. J., & Egger, R. 2000, *A&A*, 364, 935
 Brown, J. A., Sneden, C., Lambert, D. L., & Dutchover, E. 1989, *ApJS*, 71, 293
 Charbonnel, C., & Balachandran, S. C. 2000, *A&A*, 359, 563
 Cousins, A. W. J. 1976, *MmRAS*, 81, 25
 Danylewych, L. L., & Nicholls, R. W. 1974, *Proc. R. Soc. London A*, 339, 197
 da Silva, L., et al. 2006, *A&A*, 458, 609
 de Laverny, P., do Nascimento, J. D., Jr., Lèbre, A., & de Medeiros, J. R. 2003, *A&A*, 410, 937
 de Medeiros, J. R., do Nascimento, J. D., Jr., Sankarankutty, S., Costa, J. M., & Maia, M. R. G. 2000, *A&A*, 363, 239
 de Medeiros, J. R., & Mayor, M. 1999, *A&AS*, 139, 433
 do Nascimento, J. D., Jr., Charbonnel, C., Lèbre, A., de Laverny, P., & de Medeiros, J. R. 2000, *A&A*, 357, 931
 Edvardsson, B., Andersen, J., Gustafsson, B., Lambert, D. L., Nissen, P. E., & Tomkin, J. 1993, *A&A*, 275, 101
 Famaey, B., Jorissen, A., Luri, X., Mayor, M., Udry, S., Dejonghe, H., & Turon, C. 2005, *A&A*, 430, 165
 Fuhr, J. R., Martin, G. A., & Wiese, W. L. 1988, *J. Phys. Chem. Ref. Data*, 17(S4), 1
 Girardi, L., Bressan, A., Bertelli, G., & Chiosi, C. 2000, *A&AS*, 141, 371
 Golay, M. 1972, *Vistas Astron.*, 14, 13
 Gratton, R. G. 1989, *A&A*, 208, 171
 Gratton, R. G., & Sneden, C. 1987, *A&AS*, 68, 193
 ———. 1994, *A&A*, 287, 927
 Gray, D. F. 1989, *ApJ*, 347, 1021
 Gray, D. F., & Nagar, P. 1985, *ApJ*, 298, 756
 Gray, D. F., & Toner, C. G. 1986, *ApJ*, 310, 277
 ———. 1987, *ApJ*, 322, 360
 Grevesse, N., Lambert, D. L., Sauval, A. J., van Dishoeck, E. F., Farmer, C. B., & Norton, R. H. 1991, *A&A*, 242, 488
 Grevesse, N., & Sauval, A. J. 1999, *A&A*, 347, 348
 Gustafsson, B., Bell, R. A., Eriksson, K., & Nordlund, Å. 1975, *A&A*, 42, 407
 Gustafsson, B., Edvardsson, B., Eriksson, K., Mizuno-Wiedner, M., Jørgensen, U. G., & Plez, B. 2003, in *ASP Conf. Ser.* 288, *Stellar Atmosphere Modeling*, ed. I. Hubeny, D. Mihalas, & K. Werner (San Francisco: ASP), 331
 Gustafsson, B., Karlsson, T., Olsson, E., Edvardsson, B., & Ryde, N. 1999, *A&A*, 342, 426
 Hakkila, J., Myers, J. M., & Stidham, B. J. 1997, *AJ*, 114, 2043
 Heiter, U., & Eriksson, K. 2006, *A&A*, 452, 1039
 Heiter, U., & Luck, R. E. 2003, *AJ*, 126, 2015
 Houdashelt, M. L., Bell, R. A., & Sweigart, A. V. 2000, *AJ*, 119, 1448
 Iben, I., Jr. 1967a, *ApJ*, 147, 624
 ———. 1967b, *ApJ*, 147, 650
 Johansson, S., Litzen, U., Lundberg, H., & Zhang, Z. 2003, *ApJ*, 584, L107
 Kotlar, A. J. 1978, Ph.D. thesis, MIT
 Künzli, M., North, P., Kurucz, R. L., & Nicolet, B. 1997, *A&AS*, 122, 51
 Lallement, R., Welsh, B. Y., Vergely, J. L., Crifo, F., & Sfeir, D. 2003, *A&A*, 411, 447
 Lambert, D. L., & Reddy, B. E. 2004, *MNRAS*, 349, 757
 Lambert, D. L., & Ries, L. M. 1981, *ApJ*, 248, 228

- Lèbre, A., de Laverny, P., de Medeiros, J. R., Charbonnel, C., & Da Silva, L. 1999, *A&A*, 345, 936
- Lèbre, A., de Laverny, P., do Nascimento, J. D., Jr., & de Medeiros, J. R. 2006, *A&A*, 450, 1173
- Leroy, J. L. 1999, *A&A*, 346, 955
- Luck, R. E. 1977, *ApJ*, 218, 752
- . 1991, *ApJS*, 75, 579
- Luck, R. E., & Bond, H. E. 1991, *ApJS*, 77, 515
- Luck, R. E., & Challener, S. L. 1995, *AJ*, 110, 2968
- Luck, R. E., & Heiter, U. 2005, *AJ*, 129, 1063
- . 2006, *AJ*, 131, 3069
- Luck, R. E., & Wepfer, G. G. 1995, *AJ*, 110, 2425
- MacConnell, D. J., Frye, R. L., & Uppgren, A. R. 1972, *AJ*, 77, 384
- Martin, G. A., Fuhr, J. R., & Wiese, W. L. 1988, *J. Phys. Chem. Ref. Data*, 17(S3), 1
- Mashonkina, L., & Zhao, G. 2006, *A&A*, 456, 313
- McCarthy, J. K., Sandiford, B. A., Boyd, D., & Booth, J. M. 1993, *PASP*, 105, 881
- McClure, R. D. 1976, *AJ*, 81, 182
- McWilliam, A. 1990, *ApJS*, 74, 1075
- . 1997, *ARA&A*, 35, 503
- Mendoza, E. E. 1963, *Tonantzintla Tacubaya*, 3, 137
- Mermilliod, J.-C., Mermilliod, M., & Hauck, B. 1997, *A&AS*, 124, 349
- Nordström, B., et al. 2004, *A&A*, 418, 989
- Perryman, M. A. C., et al. 1997, *The Hipparcos and Tycho Catalogues* (ESA SP-1200; Noordwijk: ESA)
- Reddy, B. E., & Lambert, D. L. 2005, *AJ*, 129, 2831
- Sfeir, D. M., Lallemeunier, R., Crifo, F., & Welsh, B. Y. 1999, *A&A*, 346, 785
- Short, C. I., & Hauschildt, P. H. 2006, *ApJ*, 641, 494
- Snedden, C. 1973, Ph.D. thesis, Univ. Texas, Austin
- Sweigerart, A. V., & Gross, P. G. 1978, *ApJS*, 36, 405
- Tautvaišiene, G., Edvardsson, B., Puzeras, E., & Ilyin, I. 2005, *A&A*, 431, 933
- Unsöld, A. 1938, *Physik der Sternatmosphären, mit Besonderer Berücksichtigung der Sonne* (Berlin: Springer)
- Vergely, J.-L., Ferrero, R. F., Egret, D., & Koeppen, J. 1998, *A&A*, 340, 543
- Wallerstein, G. 1962, *ApJS*, 6, 407
- Wallerstein, G., Greenstein, J. L., Parker, R., Helfer, H. L., & Aller, L. H. 1963, *ApJ*, 137, 280
- Wolf, V. M., Tomkin, J., & Lambert, D. L. 1995, *ApJ*, 453, 660